Geological Journal

WILEY

RESEARCH ARTICLE

Unravelling the Tectonic Nature of Charnockites Across the Highland and Wanni Complexes in Northeastern Sri Lanka: Implications for Demarcating Their Uncertain Lithotectonic Boundary

P. L. Dharmapriya[1] | W. M. R. Jayathilake[1] | Lei Zhao[2] | Pahan Abewardana[1] | R. Kleinschrodt[3] | N. D. Subasinghe[4]

[1]Department of Geology, University of Peradeniya, Peradeniya, Sri Lanka | [2]Institute of Geology and Geophysics, Chinese Academy of Sciences, Beijing, China | [3]Institute for Geology and Mineralogy, University of Cologne, Cologne, Germany | [4]National Institute of Fundamental Studies (NIFS), Kandy, Sri Lanka

Correspondence: P. L. Dharmapriya (prasannad@sci.pdn.ac.lk)

Received: 18 January 2024 | **Revised:** 31 December 2024 | **Accepted:** 8 January 2025

Handling Editor: M. Satish-Kumar

Funding: This work was supported by a Program from the China–Sri Lanka Joint Center for Education and Research, Chinese Academy of Sciences (059GJHZ2024129MI), the National Research Council (NRC) Sri Lanka (Grant No: NRC 19–092) and the Peradeniya University Research Grant (Grant No. URG/18/43/S). The authors acknowledge the support of the National Natural Science Foundation of China (Grant No. W2412091) for the U–Pb zircon geochronology analysis. PLD highly acknowledges the German Academic Exchange Service (DAAD) for the grant DAAD Fellowship for Research Stay for University Academics and Scientists, 2021 (Grant No. 5755233).

Keywords: charnockites | Highland Complex | tectonic discrimination | tectonic nature | Wanni Complex

ABSTRACT

The tectonic evolution of terranes and microblocks is crucial for understanding the supercontinental cycle. Sri Lanka, centrally located between East and West Gondwana, offers insights into late Neoproterozoic continental tectonics. Ambiguities in defining boundaries between the Highland Complex (HC) and Wanni Complex (WC) of Sri Lanka prompted this study. Utilising whole-rock major and trace element geochemistry, and U–Pb zircon geochronology, we explore charnockites at the inferred HC-WC boundary, revealing their tectonic nature. Charnockites on the WC side (CWCs) display tholeiitic trends, characterised as Fe-rich, metaluminous A2-type granites. Tectonic discrimination diagrams position CWCs in the within-plate granite field. The $^{238}U/^{206}Pb$ zircon geochronology of three WC-side charnockites gave Late Neoproterozoic metamorphic ages from 576 ± 37 to 561 ± 50 Ma and middle to early Neoproterozoic protolith crystallisation ages from 1011 ± 46 to 690 ± 15 Ma. Hence, protoliths of CWCs suggest some form of extensional tectonics in a continental environment during the early to middle Neoproterozoic that played a major role in the crustal evolution of the northeastern part of the WC. Out of the collected seven charnockites in the HC side (CHCs), three samples shared geochemical signatures resembling the CWCs. The $^{206}Pb/^{238}U$ zircon ages of one of the samples yielded crystallisation age of $\sim 780 \pm 6$ Ma and, metamorphic ages from 608 ± 9 to 541 ± 16 Ma, respectively. The rest of the CHCs exhibit calc-alkaline trend, identified as Mg-rich, metaluminous, I-type granites. Tectonic discrimination diagrams reveal volcanic arc signatures, indicating a subduction-related collisional tectonic setting. Geochemical and geochronological findings, coupled with field relations and prior research, lead to the interpretation that charnockites in the northeastern HC-WC boundary possess a distinctive geodynamic history, implying involvement in two distinct tectonic settings. Presently, at the erosion surface, the north-eastern portion of the HC-WC boundary, exhibits a highly diffused nature and manifests as a mixed rock zone.

1 | Introduction

The amalgamation of supercontinents through the supercontinent cycle facilitates the vertical and horizontal growth of continental crust. Accretionary orogeny along continental margins, where the oceanic lithosphere subducts beneath the continental crust, is one of the significant products of the supercontinent cycle. These regions act as primary sites for the addition of juvenile continental crust (Condie et al. 2007). Accretionary orogens have likely been active throughout much of Earth's history and serve as major sites for continental growth and preservation as mountain belts during one or more tectonothermal events (orogenies), ultimately stabilising and cratonizing the orogeny (Cawood, Kroner, and Pisarevsky 2006). Petrologists are interested in studying the terrane boundaries and tectono-metamorphic evolution of individual lithotectonic units within these accretionary orogenic belts, as they provide vital clues for understanding the crustal evolution.

The Precambrian crust of Sri Lanka is considered as a part of a cratonized paleo-accretionary orogenic belt formed simultaneously with the amalgamation of Gondwana (e.g., Kröner, Cooray, and Vitanage 1991; Kröner et al. 1991; Kehelpannala 2004; Santosh et al. 2014). The Sri Lankan basement has been subdivided into four major lithotectonic units: the Wanni Complex (WC), the Highland Complex (HC), the Vijayan Complex (VC) and the Kadugannawa Complex (KC) (Kröner, Cooray, and Vitanage 1991; Kröner et al. 1991; Cooray 1994), as shown in Figure 1a,b. These subdivisions are based on Nd-model ages, U–Pb zircon ages and regional structural interpretations (Milisenda et al. 1988, 1994; Kröner et al. 1987a, 1987b, 1991; Kröner, Cooray, and Vitanage 1991; Kehelpannala 1991, 2003, 2004; Kleinschrodt, Voll, and Kehelpannala 1991; Kriegsman 1994). Advancements in U–Pb and Lu–Hf zircon geochronology and Nd model ages have indicated that the HC and WC have distinct geological histories prior to their amalgamation during the late Neoproterozoic

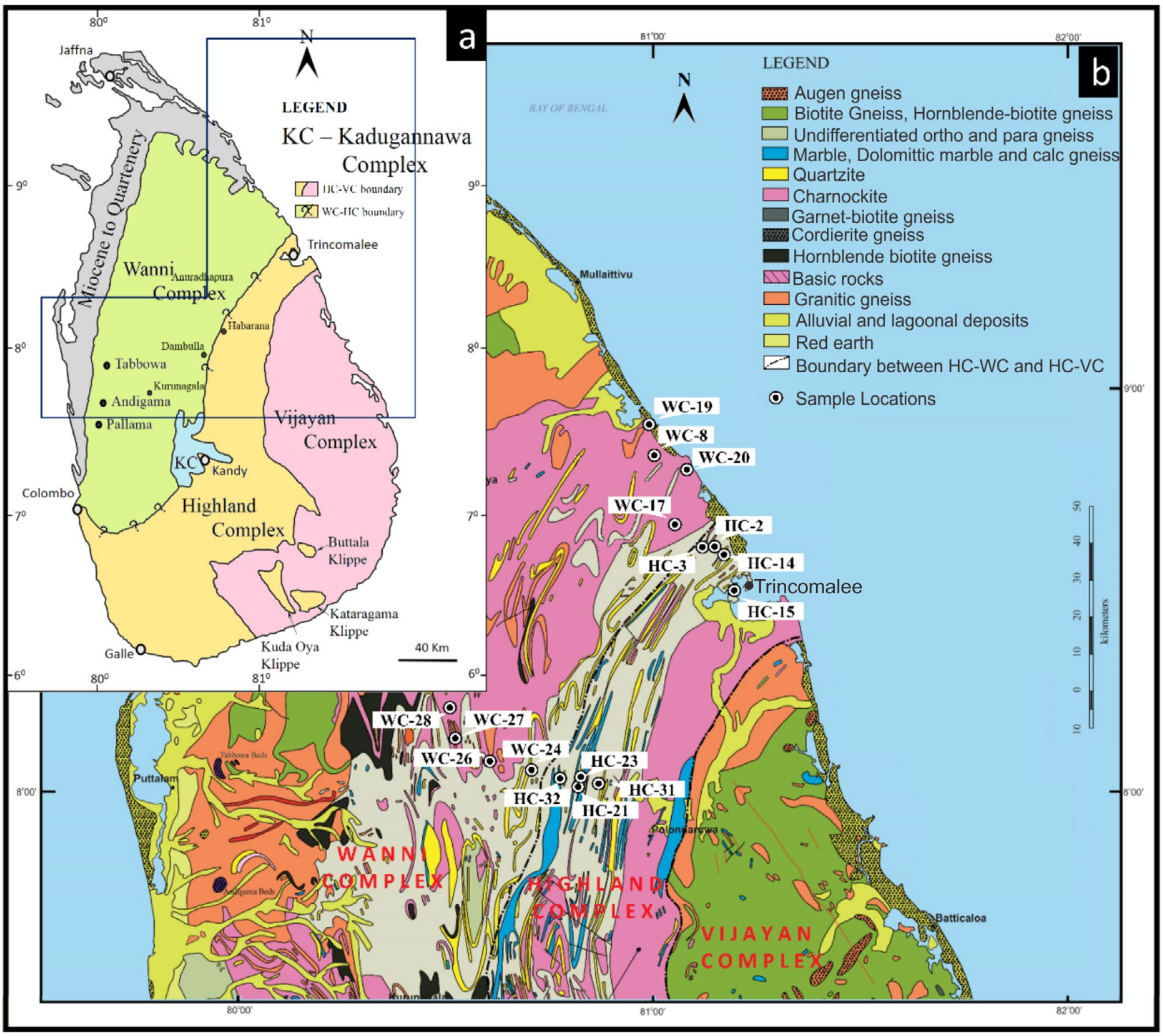

FIGURE 1 | (a) Major litho-tectonic subdivisions of Sri Lanka (Litho-tectonic units after Kröner, Cooray, and Vitanage 1991; Kröner et al. 1991 and Cooray 1994) (b) Geological map of study area showing sampled localities (Geology Map After National Atlas of Sri Lanka, 2007).

(e.g., Malaviarachchi 2018; Kitano et al. 2018; Santosh et al. 2014; Milisenda et al. 1988). Another significant tectonic boundary in Sri Lanka, between the HC and VC, has been interpreted as a low-angle thrust/shear contact that is geologically well-stabilised (Hatherton, Pattaratchi, and Ranasinghe 1975; Vitanage 1985; Voll and Kleinschrodt 1991). The boundary between the KC and the HC in central Sri Lanka is well-defined lithologically, contrasting in metamorphic grade, geological structure, Nd model ages, Pb isotopic discriminations and U–Pb zircon geochronology (e.g., Cooray 1994).

The currently accepted boundary between the HC and WC was determined by Kröner et al. (Kröner, Cooray, and Vitanage 1991; Kröner et al. 1991) based on lithologies and structural aspects, along with Nd model ages (Milisenda et al. 1988), Pb isotopic discriminations (Liew, Milisenda, and Hofmann 1991) and U–Pb zircon ages of metaigneous and metasedimentary rocks (Hölzl et al. 1991). However, the position of the southwestern and northeastern HC-WC boundaries remains controversial due to a lack of detailed geochemical, geochronological, structural and petrological studies. The southwestern boundary of the country cross-cuts the structural trends of geological structures (e.g., general foliation, and the axial planes of antiform and synform structures) and is defined primarily based on Nd model ages (Milisenda et al. 1988). The limitations of using only Sm-Nd model ages for such interpretations have been discussed by many researchers (e.g., Hölzl et al. 1994; Perera and Kagami 2011). In contrast, the section between HC and WC from the northern part of Kandy to Habarana (Figure 1a), in the central part of the country, has been more or less fixed (Kehelpannala and Ranaweera 2007; Ranaweera and Kehelpannala 2019). Due to the presence of mesoscopic to microscopic scale shear sense indicators such as S–C′ fabrics, δ-type and σ-type asymmetric objects, asymmetric folds, rotated garnet porphyroblasts, sheath folds and strip gneisses along the proposed HC-WC boundary from north of Kandy to Habarana (Figure 1a), some researchers have interpreted the HC-WC boundary as a lower crustal ductile shear zone (Kehelpannala 1997; Ranaweera and Kehelpannala 2019). In contrast, the northeastern part of the boundary between the two complexes is highly uncertain, and the nature of the boundary in this region is not yet fully understood. Charnockites and granitic gneisses are intercalated with metasediments in the area, and their tectono-metamorphic evolution has not yet been studied.

Recent advancements in U–Pb geochronology of metaigneous rocks in the central and southwestern parts of both HC have indicated discrete protolith emplacement ages of approximately 2500 Ma, 1950–1800 Ma, 850–670 Ma and ~580 Ma (e.g., Hölzl et al. 1994; Sajeev et al. 2007; Santosh et al. 2014; He et al. 2016; Kitano et al. 2018; Zhao et al. 2023). The WC metaigneous rocks have shown main magmatic pulses around 1100–860 Ma, 790–750 Ma and 580 Ma (Hölzl et al. 1994; Kröner, Kehelpannala, and Hegner 2003; Santosh et al. 2014; He et al. 2016; Kitano et al. 2018). Thus, both complexes contain protoliths with Middle to Late Neoproterozoic ages (e.g., Kitano et al. 2018).

Jayathilake et al. (2023) studied the metamorphic evolution of charnockites (the samples used in this study) across the lithotectonic boundary between the HC and the WC in the northeastern part of the country. They concluded that there is no evidence of contrasting metamorphic evolution of charnockites across the inferred HC-WC boundary in the study area. However, earlier researches have indicated that the geochemical signatures of metaigneous and metasedimentary rocks in the HC and WC have yielded distinct protolith signatures (e.g., Pohl and Emmermann 1991; Pram and Pohl 1994; Santosh et al. 2014; He et al. 2016). Notably, Prame (1997) highlighted that charnockites in the southern part of the HC exhibit two distinct geochemical signatures, further emphasising the complexity of their origin. Consequently, relying solely on U–Pb geochronology or geochemical signatures to demarcate the uncertain lithotectonic boundary in the northeastern HC-WC region is potentially insufficient. Therefore, a combined approach using both U–Pb geochronology and whole-rock geochemical analyses of charnockites across the HC-WC boundary would be highly beneficial for reducing the complexity in delineating the boundary between these two lithotectonic complexes.

Building on this hypothesis, we studied the geochemical signatures and U–Pb zircon geochronology of charnockite across the northeastern part of the HC-WC inferred boundary to determine their protolith signatures and tectonic nature, including the tectonic settings at which the protoliths were emplaced. Additionally, we re-examined the geographical position of the northeastern end of the boundary around Trincomalee (Figure 1a), where the uncertain boundary has been primarily inferred in previous studies through a few Nd model age data points and geological mapping.

2 | Geological Background

2.1 | General Geology of the HC and WC

The HC is a broad belt of rocks extending from the northeast to the southwest between the WC and the VC through the central highlands of the country. It is primarily composed of granulitic supracrustal rocks, including garnet sillimanite gneisses, quartzites, marbles and calc-silicate rocks. Additionally, orthogneisses of largely granitoid composition and charnockitic rocks are present (Cooray 1994; Santosh et al. 2014).

Across the HC, metamorphic temperatures and pressures increase from 600°C to 850°C and 5–7 kbar in the southwest to 800°C–900°C and 8–10 kbar in the central part and toward the east (Kröner and Williams 1993; Raase and Schenk 1994; Dharmapriya et al. 2014, 2017b, 2020). Ultra-high temperature (UHT) granulites have been reported in the central HC and rarely in the southwestern part, experiencing extreme crustal metamorphism at 900°C–1150°C and 9–12.5 kbar (Kriegsman and Schumacher 1999; Osanai et al. 2006; Sajeev and Osanai 2004a, 2004b; Sajeev et al. 2007; Malaviarachchi and Dharmapriya 2015, 2021; Dharmapriya et al. 2017a, 2021; Dharmapriya, Kriegsman, and Malaviarachchi 2021; Martin, Schumann, and Dharmapriya 2022).

Whole-rock Nd isotopic data indicate that the rocks in the HC were mainly derived from Late Archean to Paleoproterozoic sources (3200–2000 Ma; Milisenda et al. 1988, 1994). The detrital zircon spectrum extends from 3500 to 703 Ma (Kröner et al. 1987a, 1987b; Hölzl et al. 1991, 1994; Sajeev, Williams, and Osanai 2010; Dharmapriya et al. 2015, 2016; Takamura et al. 2016; Kitano et al. 2018). The protolith of the orthogneisses in the HC was emplaced mainly in four episodes: around ~2500 Ma, 1950–1800 Ma, 850–670 Ma and ~580 Ma (Kröner and Williams 1993; Hölzl et al. 1994; Sajeev et al. 2007; Kitano et al. 2018; Zhao et al. 2023). The peak granulite facies metamorphism of the complex is suggested to have occurred around 610–530 Ma (e.g., Kröner et al. 1987a, 1987b; Hölzl et al. 1991, 1994; Sajeev, Williams, and Osanai 2010; Dharmapriya et al. 2015, 2016; Takamura et al. 2016; Kitano et al. 2018).

The WC, formerly termed the Western Vijayan Complex, is situated west and northwest of the HC. It is predominantly composed of upper amphibolite to granulite facies orthogneisses and minor metasedimentary rocks (Cooray 1994). Metaigneous rocks of the WC consist of a range of compositions, including granitic, granodioritic, monzonitic, tonalitic, charnockitic and enderbitic rocks, reflecting varying protolith chemistries (Pohl and Emmermann 1991). The western part of the WC includes less deformed granites, including the post-tectonic K-feldspar-rich granite of Thonigala (Hölzl et al. 1991; Cooray 1994) and carbonatite (e.g., Pitawala et al. 2003; Wang et al. 2021; Su et al. 2022). Migmatitic rocks are also present in many places in the WC. The peak metamorphic conditions of the WC have been suggested to be 700°C–830°C and 5–7 kbar (Raase and Schenk 1994; Santosh et al. 2014; Hirayama et al. 2020). The WC yields Nd-model ages of 2000–1000 Ma (Milisenda et al. 1988, 1994). The intrusion ages of Wanni gneisses are mainly around 1100–860 Ma, 790–750 Ma and around 580 Ma (Kröner, Jaeckel, and Williams 1994; Kröner, Kehelpannala, and Hegner 2003; Hölzl et al. 1994; Santosh et al. 2014; He et al. 2016). Detrital zircon yielded ages of 2700–750 Ma (Hölzl et al. 1994; Takamura et al. 2016). Peak metamorphism occurred around 590–540 Ma (Kröner, Jaeckel, and Williams 1994; Kröner, Kehelpannala, and Hegner 2003; Hölzl et al. 1994; Santosh et al. 2014; He et al. 2016). The unmetamorphosed granite at Tonigala and Galgamuwa yielded an age of 550 Ma (Hölzl et al. 1991). The in situ charnockitization in the WC occurred at 535 Ma, post-dating the peak granulite facies metamorphism (Burton and O'Nions 1990).

Munasinghe and Dissanayake (1980) investigated the trace-element geochemistry of charnockites in the HC, revealing that the chemistry of intermediate to basic charnockites indicates an approximately basaltic composition. These basaltic-nativity charnockites and the amphibolites in the HC are suggested to be the result of the metamorphism of volcanic basalts. Dissanayake and Munasinghe (1984) argued that the charnockites and related rocks of the present HC and the westernmost part of the WC correspond to an igneous differentiation sequence of basaltic composition. Pohl and Emmermann (1991) pointed out that granulite facies metabasites, charnockites and rare enderbites constitute a major portion of the HC, while the WC represents a bimodal basalt-rhyolite association.

Prame (1997) classified charnockites in southern Sri Lanka into two compositional groups: granitic and tonalitic. Tonalitic rocks were interpreted to have formed in an orogenic setting with a thickened crust under compressive tectonic conditions, exhibiting calc-alkaline characteristics typical of volcanic-arc magmas within a convergent plate setting. Their intermediate to felsic composition (SiO_2 ~55%–75%) and compositional diversity were attributed to an arc environment underlain by continental crust. In contrast, the granitic charnockites displayed geochemical traits of A-type granites, suggesting derivation from ancient felsic crust subjected to prior subduction or collisional magmatism. These granitic rocks likely emplaced in an extensional or post-collisional environment, possibly linked to trans-tensional tectonics, yet they show distinctions from granites formed in true anorogenic settings. The study proposed that tectonic processes during the Pan-African Orogeny may have juxtaposed rock suites of differing origins or involved a transition in tectonic regimes.

Santosh et al. (2014) reported the arc signature of magmatic suites in the WC, identified using trace and rare earth element patterns and the Rb-Y-Nb and Rb-Yb-Ta discrimination plots. They argued that these metaigneous rocks originated from felsic to intermediate arc magmas, and the volcanic arc affinity for mafic granulites represents subduction-related mafic magmatism. Furthermore, those authors reported that mafic blocks incorporated into metasedimentary rocks of the HC show N-MORB signatures, that is, oceanic island alkali basalt affinity. This suggests the accretion of remnants of the oceanic lithosphere during the subduction-collisional event of the HC. He et al. (2016) pointed out that the studied felsic suite of the HC and WC shows a calc-alkaline affinity and is derived from arc-related magmas, with a composition consistent with an origin in a continental arc. Pohl and Emmermann (1991) also noted that the granitic and syenitic gneisses and late- to post-tectonic granites in the WC exhibit typical chemical characteristics of A-type granitoids.

2.2 | The Kadugannawa and the Vijayan Complexes

The KC is exposed in doubly plunging upright folds around Kandy in the central part of the country, formerly known as 'Arenas' (Vitanage 1972; Almond 1991). It yields Nd-model ages ranging between 1800 and 1100 Ma (Milisenda et al. 1988, 1994). This complex mainly comprises hornblende- and biotite-bearing orthogneisses, gabbros, diorites, granodioritic to granitic gneisses, charnockites, enderbites and minor metasediments that have undergone metamorphism under upper amphibolite to granulite facies conditions (Kriegsman 1994; Kröner, Kehelpannala, and Hegner 2003; Willbold et al. 2004; Santosh et al. 2014).

The dominantly upper amphibolite facies VC yields Nd-model ages in the range of 3300–1100 Ma (Milisenda et al. 1988, 1994; Malaviarachchi, Satish-Kumar, and Takahashi 2021). This complex mainly consists of microcline-bearing granitic gneisses, augen-gneisses, migmatites and hornblende-biotite gneisses (Cooray 1984; Kehelpannala 1997; Madhavan et al. 1998; Kröner et al. 2013a, 2013b). Rare sedimentary enclaves, such as quartzite, calc-silicate rocks and marble, have also been reported (Dahanayake 1982; Dahanayake and Jayasena 1983).

2.3 | Nature of the Boundary Between Highland and Wanni Complexes

According to tectonic interpretations, some authors suggest that the crustal units in the Sri Lankan Basement evolved independently before amalgamating during the assembly of Gondwana (Kehelpannala 1997, 2003; Kröner, Kehelpannala, and Hegner 2003). In these models, the HC is viewed as a Paleoproterozoic microcontinent of unknown origin that collided with the WC and VC arcs through two distinct collision events. Santosh et al. (2014) proposed a model of double-sided subduction, suggesting that the WC in the west and the VC in the east represent continental and magmatic arcs, respectively. The collision of these arcs formed a suture referred to as the HC. However, the double-sided subduction model was revised by Malaviarachchi (2018) and Satish-Kumar et al. (2021), who proposed a 'two-staged subduction' concept involving non-coeval arc segments of the WC and VC.

Historically, the boundary between the HC and WC has been poorly defined (Figure 2a–c). Although geochemical and isotopic data provide useful information on the geographical position and geological origin, there is no consistent structural boundary between these crustal units (Kleinschrodt, Voll, and Kehelpannala 1991). Metasediments, charnockitic rocks formed under granulite conditions, pelitic gneisses, hornblende-bearing metagranitoids and marbles are observed along the inferred margin of the HC-WC (Kehelpannala and Ranaweera 2007). Figure 2a shows the suggested lithotectonic subdivision after Vitanage (1959). In 1978, Cooray revised this boundary based on metamorphism and lithology, considering it a lithostratigraphic boundary (Cooray 1978, 1984; Figure 2b). The boundary between the western Vijayan (now the WC) and the Highland Group was then positioned north of Bingiriya, west of Maho and Anuradhapura, and west and north of Vavuniya (Figure 2c; Cooray 1982). The northern part of this boundary was later adjusted by Cordani and Cooray (1990). Milisenda et al. (1988) and Kröner et al. (Kröner, Cooray, and Vitanage 1991; Kröner et al. 1991) suggested placing the boundary between the WC and HC, west of Habarana, based on Ndmodel ages and zircon ages, respectively. Subsequent studies have largely confirmed this boundary. Kehelpannala (1991) proposed the HC-WC boundary as a tectonic boundary based on structural features, lithology, metamorphic grade and isotopic ages. Later works recorded this boundary as a granulite facies sub-horizontal crustal shear zone occurring within convergent tectonic plates (Kehelpannala 1997, 2003). Cooray (1994) used isotopic data from Milisenda et al. (1988) to shift the western end of the margin to north of Colombo and west of Kurunegala and Dambulla (Cooray 1994). Kehelpannala (2003) argued that Grenvillian (~791–755 Ma) ductile deformation occurred in the WC, but these structures were not reported in the HC. The reported structures were formed during two separate collisional events: the first between the HC microplate and the WC arc, resulting in granulite-facies deformation and the second between the HC-WC module and the VC arc, causing upper-amphibolite metamorphism and migmatization in the VC (Kehelpannala 1997). Deformation structures in both HC and WC include E-W stretching lineation, closely spaced foliation and folds (Kehelpannala 2003), while non-coaxial deformation contributed to asymmetric structures in the WC (Kriegsman 1995; Tani 1997).

Berger and Jayasinghe (1976) first suggested that the Sri Lankan basement has undergone at least three deformation phases, labelled D1 to D3. The D1 and D2 phases were responsible for creating the major lineations and foliations (L-S fabric), including the principal compositional layering. The D3 phase resulted primarily in the formation of large-scale upright folds during the upliftment. Subsequent studies (e.g., Kehelpannala 1997; Kleinschrodt 1994; Kriegsman 1994, 1995; Tani and Yoshida 1996) provided evidence for additional deformation events or stages (see Dharmapriya, Kriegsman, and Malaviarachchi 2021). The syn-tectonic D2 event was particularly significant in forming the major lineation and foliation

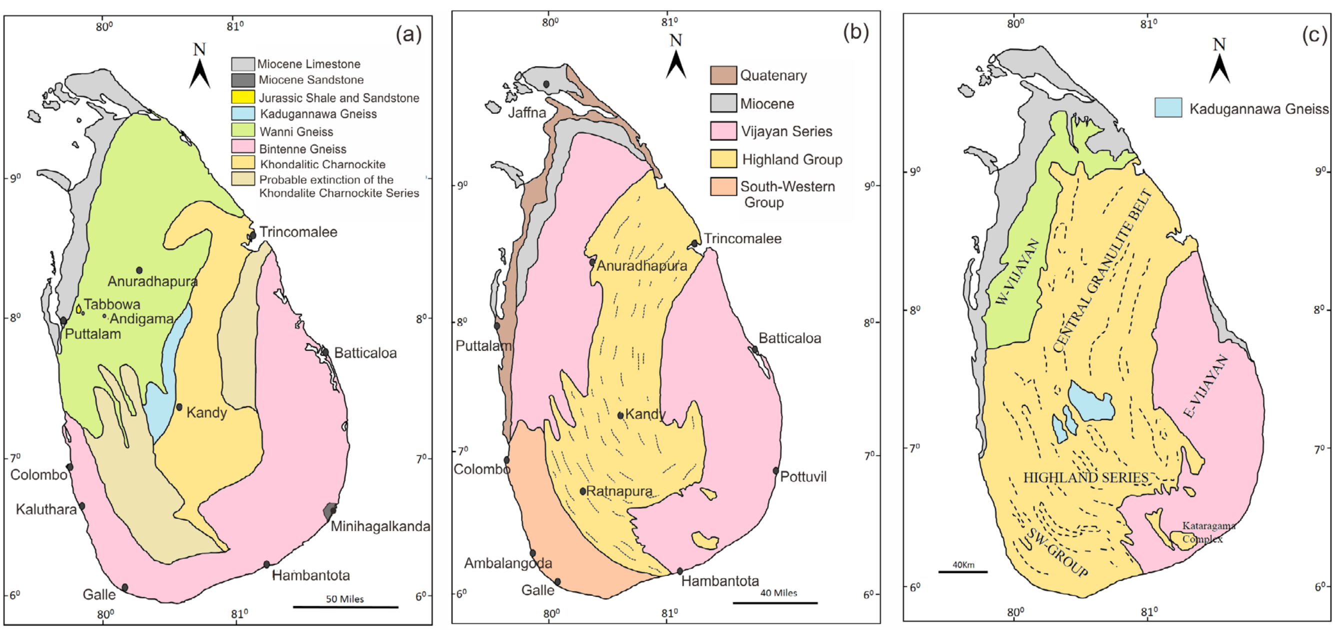

FIGURE 2 | Some of the previous subdivisions of the Precambrian crust of Sri Lanka (a) after Vitanage (1959), (b) after Cooray (1978) and (c) after Voll and Kleinschrodt (1991).

(L-S fabric), resulting in the main compositional layering of both the HC and the WC (e.g., Berger and Jayasinghe 1976; Kehelpannala 1997). During the D2 deformation, the transitional collision between the WC and HC occurred, with the WC thrusting over the HC microplate in a NNW–SSE direction (Tani 1997; Kehelpannala 2003; Ranaweera and Kehelpannala 2019). Detailed structural geological studies by Kehelpannala and Ranaweera (2007), Ranaweera (2008) and Ranaweera and Kehelpannala (2019) have refined the geographical position of the HC-WC boundary in the central part of the country.

However, due to insufficient detailed geochemical, geochronological, structural and petrological studies, the positions of the southwestern and northeastern HC-WC boundaries remain poorly defined, and these boundaries are still considered inferred (Cooray 1994; Santosh et al. 2014; He et al. 2016).

3 | Sample Descriptions and Field Relations

Samples were collected from two separate traverses across the inferred boundary between the HC and WC. Traverse 1 extended from Trincomalee (sample location HC-15) to Pulmuddai (sample location WC-19), while Traverse 2 extended from Minneriya (sample location HC-31) to Maradankadawala (sample location WC-28), as illustrated in Figure 1b. Fresh samples were obtained from quarries and road cuts, with a focus on charnockite and associated lithologies. Table S1 summarises the collected rock types and sampling localities. Jayathilake et al. (2023) provided a detailed description of the petrography, mineral chemistry and P–T evolution for samples HC-2, HC-3, HC-14, HC-15, WC-8, WC-17, WC-19, WC-20, WC-26 and WC-28 (see Figure 1a). They reported that these charnockites experienced peak metamorphic conditions with temperatures reaching approximately 750°C–800°C. Following the peak metamorphism, a near-isobaric cooling (IBC) stage was suggested for both HC and WC charnockites. Figure 3 displays field images of selected locations.

The majority of charnockite samples from both the HC and WC are massive (see Figure 3 for descriptions). These charnockites exhibit a typical greasy lustre (Figure 3a–h). Some samples feature clusters of hornblende-pyroxenes and biotite flakes, while others show a uniform distribution of minerals with very fine grains. Partial melt patches are commonly observed, containing substantial quartz, feldspars, hornblende, or orthopyroxene grains (e.g., HC-2, HC-3). Although most rocks have a granular, massive appearance, biotite flakes are randomly oriented and medium-grained orthopyroxene occasionally defines a weak lineation (e.g., WC-8), which may be subtle in hand specimens.

In some locations (e.g., HC-2, HC-3), biotite, hornblende and two-pyroxene-rich mafic layers or blocks are interlayered with charnockitic rocks. These mafic layers vary from a few millimetres to 8–15 cm in thickness (Figure 3c) and extend parallel to the weak foliation within the massive rock. Similarly, quartzite bands approximately 2–5 cm thick are interlayered with charnockitic rock in other locations (e.g., HC-21, HC-23). In some areas (e.g., WC-8), quartz veins are present, oriented both parallel and oblique to the foliation.

Occasionally, charnockites are associated with hornblende-biotite gneisses where the contact between the two lithologies is gradational (e.g., HC-2, HC-3). This study further examines the petrography of the studied charnockites, including samples HC-21, HC-31 and HC-32 (see Figure 1a). Charnockites collected from the HC side of the inferred HC-WC boundary, as defined by Kröner et al. (Kröner, Cooray, and Vitanage 1991; Kröner et al. 1991), are referred to hereafter as 'CHCs' (Charnockite-Highland Complex Side). Also the charnockites collected from the WC side of the inferred HC-WC boundary, as delineated by Kröner et al. (Kröner, Cooray, and Vitanage 1991; Kröner et al. 1991), are referred to as 'CWCs' (Charnockite-Wanni Complex Side). The CHCs mainly comprise quartz, alkali feldspar, plagioclase, orthopyroxene, clinopyroxene and hornblende (Figure 4a–d). Some samples, such as HC-3, also contain primary biotite grains. Opaque (ore) minerals, including ilmenite and magnetite, are abundant in many samples (e.g., HC-3, HC-14, HC-15) and contribute to variations in overall composition. Minor and accessory minerals include zircon (Figure 1d) and ore minerals, with apatite also present as an accessory phase, distributed unevenly (e.g., HC-21, HC-15). Secondary minerals such as hornblende, biotite and chlorite are found in certain samples (e.g., HC-15, HC-21, see Figure 4b).

The matrix of nearly all CHCs consists of subidioblastic and xenoblastic fine- to medium-grained quartz, alkali feldspar and plagioclase, exhibiting an interlobate texture (see Figure 4a,b,d; locations HC-14, HC-15, HC-21, HC-31 and HC-32). In some locations (e.g., HC-2, HC-3), a granoblastic texture is also observed (Figure 4a,d). Subidioblastic porphyroblasts of mafic minerals, displaying sharp and uneven dissolved contacts, are common and uniformly distributed within the matrix (e.g., HC-3, HC-14, HC-15). Occasionally, grains exhibit a cumulative texture with clusters of pyroxenes and hornblende (e.g., HC-2, HC-21, HC-32). Foliation is characterised by elongated mafic minerals forming aggregates (e.g., HC-2, HC-21, HC-32; Figure 4b). Dominant mineral assemblages under peak metamorphic conditions are likely include Opx + Cpx + Kfs + Pl + Qz + Ilm ± Hbl ± Bt.

The CWCs are predominantly composed of quartz, alkali feldspar, plagioclase, orthopyroxene and opaque minerals (primarily ilmenite and magnetite) as minor phases (see Figure 4e–i). Clinopyroxene and hornblende are occasionally present, and garnet is found in certain locations (WC-19, WC-20). Common accessory minerals include allanite, apatite and zircon. Overprinted hornblende and biotite frequently replace pyroxenes.

The grain size of the constituent minerals typically ranges from medium to fine (3–0.2 mm), with some samples exhibiting very fine grains and significant grain size variation (e.g., WC-27, WC-28). Most samples display subidioblastic to xenoblastic interlobate matrix grains (Figure 4f,h), while coarse-grained, irregularly shaped xenoblastic grains are present in some locations (e.g., WC-8, WC-26). Xenoblastic porphyroclasts of clinopyroxene, hornblende and orthopyroxene exhibit sharp cleavages, although these are slightly diminished due to later alterations (Figure 4f). These grains are not associated with mafic mineral accumulations (e.g., WC-26, WC-27, WC-28). Foliation is typically defined by the alignment of

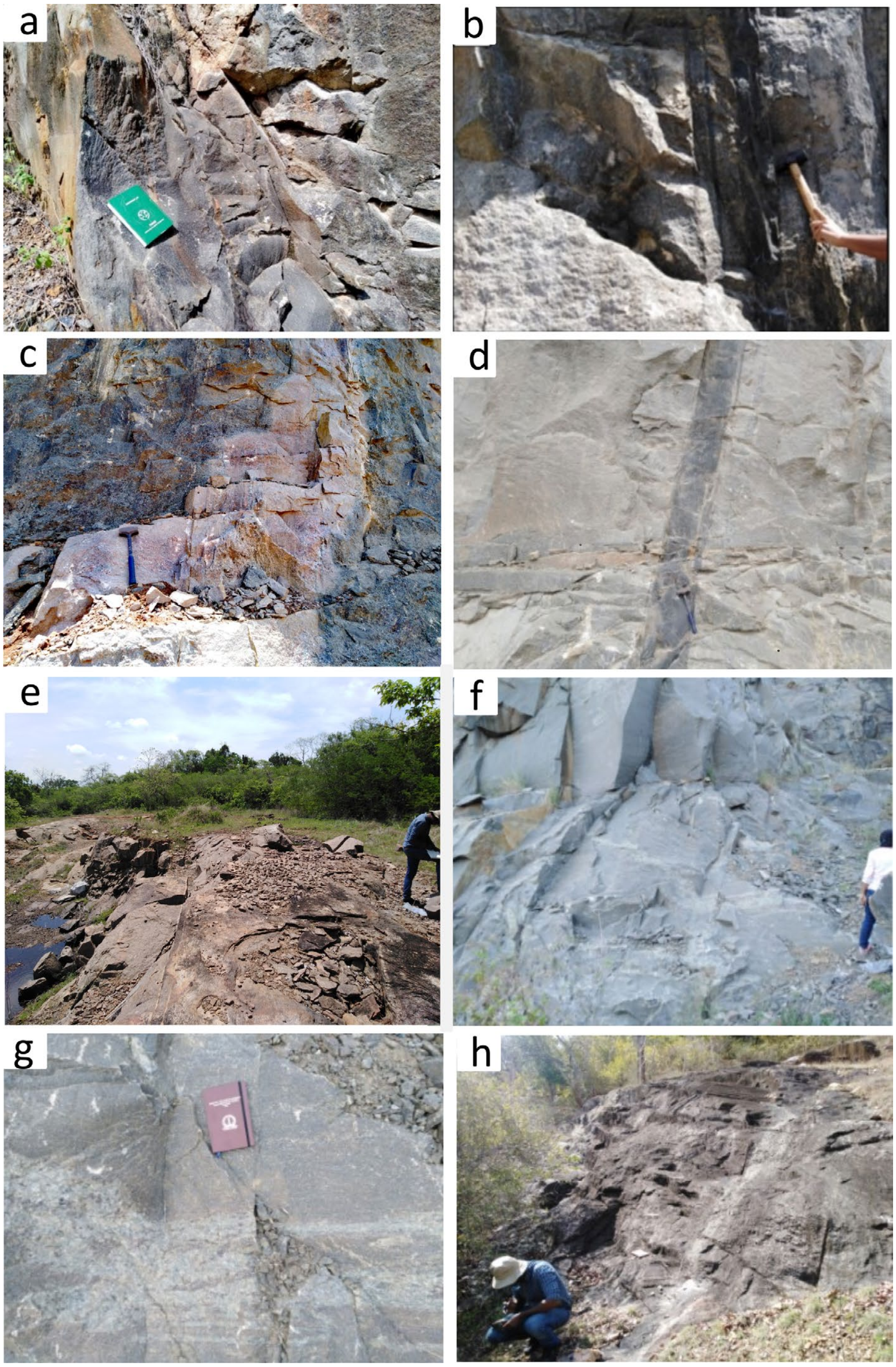

FIGURE 3 | Representative field photographs in selected study area: (a) A fresh massive charnockite at location HC-2 (photo after Jayathilake et al. 2023); (b) Interlayered mafic band (width about 10 cm) in charnockite at HC-3; (c) Interlayered microcline-rich felsic band in charnockite at HC-3 (photo after Jayathilake et al. 2023); (d) Occurrence of interlayered mafic band (about 45 cm thick) in charnockite at WC-26; (e) Massive fresh charnockite exposure at a quarry in WC-26 (photo after Jayathilake et al. 2023); (f) Massive fresh charnockite exposure in a quarry at WC-24; (g) Fresh charnockitic exposure in WC-28. The upper part of the rock appears to be the residual portion, while the lower part contains partial melt patches. (h) Fresh charnockitic exposure in WC-27.

elongated mafic minerals (clinopyroxene, hornblende and orthopyroxene) and felsic minerals (quartz, alkali feldspar and plagioclase), except in a few samples (e.g., WC-17, WC-28). Other samples show a preferred orientation of orthopyroxene and clinopyroxene (e.g., WC-8, WC-26). The peak metamorphic assemblages identified in WC charnockites include Opx + Kfs + Pl + Qz + Ilm ± Cpx ± Hbl ± Grt.

4 | Whole-Rock Chemistry

Fresh samples with homogeneous mineral distribution were selected for whole-rock major and trace element analysis. The chosen samples were cut into slabs approximately 10 cm × 5 cm × 1 cm in size. Only rock slabs devoid of surface alteration or weathering were used for geochemical analyses. The

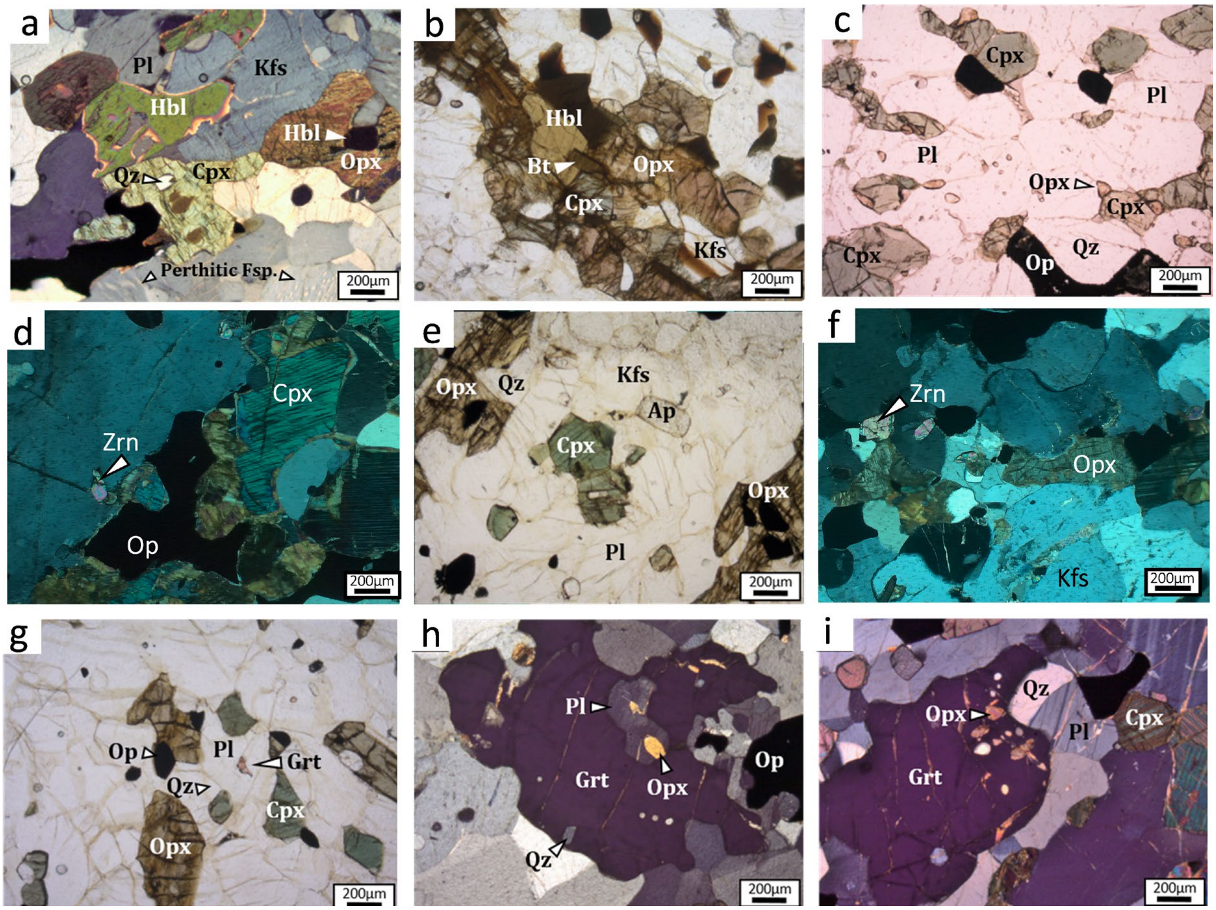

FIGURE 4 | (a) Hornblende-quartz coexisting inclusions observed in a clinopyroxene grain associated with orthopyroxene and plagioclase, indicating the reaction Hbl + Qz → Cpx + Opx + Pl + V (HC-14, Jayathilake et al. 2023), (b) both biotite and hornblende were found as inclusions in pyroxenes indicating possible dehydration reaction Bt + Hbl + Qz → Cpx + Opx + Pl + Kfs + V in HC-21 (Jayathilake et al. 2023), (c) Fine-grained orthopyroxene along the grain boundary is relatively coarse-grained clinopyroxene under the presence of quartz and plagioclase in HC-2 representing the solid–solid net transfer reaction: Cpx + Qz → Opx + Pl + Ilm (Jayathilake et al. 2023), (d) Subhedral zircon grain adjacent to subidioblastic clinopyroxene and opaque mineral in HC-21, (e) xenoblastic porphyroblasts of clinopyroxene (WC-17, Jayathilake et al. 2023), (f) euhedral and subheadral zircon grain under the presence of orthopyroxene and orthoclase in WC-19, (g) tiny xenomorphic grains of garnet were found as inclusions in some medium- to coarse-grained hypidiomorphic plagioclase which are surrounded by two pyroxenes and opaque minerals in WC-17, (h) and (i) orthopyroxene and plagioclase inclusions in garnet under the presence of quartz in WC-20 indicating the reaction Opx + Pl → Grt + Qz (Jayathilake et al. 2023).

samples were analysed in the laboratory of Actlabs, Ontario, Canada, following Code 4 of the Litho package (option 4B 1) (http://www.actlabs.com/).

The samples were fluxed using lithium metaborate and lithium tetraborate, followed by digestion with a 5% nitric acid solution. Major elements, along with Ba, Sr., Y, Zr, Be, Sc and V, were analysed using an ICP (Varian Vista 735 ICP). All other elements were analysed by ICP-MS, with the fused sample being diluted and analysed by Perkin Elmer Sciex ELAN 6000, 6100, or 9000 ICP/MS. Loss on ignition was measured by heating powdered samples for 2 h at 1050°C. Geochemical data, including major, minor trace and rare earth elements for 17 samples from both HC and WC, relative to the inferred HC-WC boundary, are presented in Table 1.

4.1 | Major Elements

The SiO_2 contents in CHCs range from approximately 52.5 wt.% to 69.3 wt.%, while CWCs exhibit SiO_2 contents from 59.5 wt.% to 73.3 wt.%. The low silica content in this sample HC-31 is likely due to the inclusion of more mafic minerals (such as pyroxene) and feldspar-rich, quartz-poor portions during sample selection for geochemical analysis.

The Al_2O_3 content in the studied samples range from 12.0 wt.% to 16.0 wt.% in CHCs and 13.4 wt.% to 16.6 wt.% in CWCs. Although, the FeO content shows no significant difference between CHCs (5.51 wt.%–11.49 wt.%) and CWCs (3.21 wt.%–10.31 wt.%), MgO contents in CHCs are relatively higher, ranging from 1.5 wt.% to 5.2 wt.%, compared to CWCs, which range from 0.2 wt.% to 1.4 wt.%.

The CaO content across all samples range from 2.85% to 4.69%. The CaO and K_2O concentrations display contrasting distributions. CHCs have CaO compositions between 3.8 wt.% and 9.8 wt.% and K_2O contents ranging from 1.5 wt.% to 5.1 wt.%, with most samples concentrated between 1.5 wt.% and 3.2 wt.%. In contrast, CWCs have CaO and K_2O concentrations ranging from 1.2 wt.% to 4.3 wt.% and 3.5 wt.% to 6.2 wt.%, respectively.

TABLE 1 | Whole-rock major, minor and rare earth element abundances of selected samples from both HC and WC.

	HC-2	HC-3	WC 8	HC-14	HC-15	WC-17	WC-19	WC-20	HC-21	WC-24	WC-26	WC-27	WC-28	HC-31	HC-32	Detection limit	
Wt.%																	
SiO_2	62.36	65.04	66.3	60.91	69.25	61.84	60.47	59.45	62.61	66.88	73.24	64.38	69.38	52.53	56.47	0.01	
Al_2O_3	15.97	15.58	14.43	15.43	11.95	13.44	15.61	16.55	15.27	14.65	12.86	15.9	14.23	14.58	15.75	0.01	
$Fe_2O_3^{(T)}$	6.92	5.51	5.50	8.48	7.04	10.31	9.37	8.51	6.05	5.79	3.21	6.32	4.48	11.49	9.37	0.01	
MnO	0.145	0.115	0.104	0.175	0.081	0.119	0.251	0.236	0.078	0.104	0.06	0.154	0.103	0.174	0.142	0.001	
MgO	0.93	1.54	0.52	1.16	0.48	1.40	0.39	0.56	2.43	0.19	0.41	0.23	0.32	5.23	2.71	0.01	
CaO	3.11	4.34	2.11	3.51	1.82	4.29	3.10	3.45	4.70	1.62	1.19	1.96	1.48	9.82	3.84	0.01	
Na_2O	4.61	3.97	3.86	4.69	2.83	2.95	4.36	4.35	3.61	4.10	3.67	4.41	3.11	3.67	3.46	0.01	
K_2O	4.00	2.89	4.85	3.74	5.06	3.53	4.41	4.54	2.89	5.58	4.93	6.15	5.92	1.50	3.24	0.01	
TiO_2	0.927	0.441	0.567	1.054	0.759	1.489	0.687	0.845	0.693	0.448	0.394	0.594	0.464	1.394	1.945	0.001	
P_2O_5	0.29	0.13	0.14	0.34	0.2	0.56	0.16	0.22	0.32	0.06	0.06	0.10	0.08	0.17	0.27	0.01	
LOI	0.25	1.12	0.82	0.01	0.34	−0.28	−0.12	−0.23	0.24	0.30	0.15	0.18	0.10	0.03	2.71		
Total	99.52	100.7	99.2	99.5	99.82	99.66	98.68	98.48	98.9	99.72	0.16	100.4	99.67	100.6	99.91		
ppm																	
Sc	15	13	11	17	10	18	50	22	13	5	4	13	8	36	17	1	
Be	2	2	3	2	3	2	2	2	3	3	3	1	1	2	3	1	
V	39	85	19	42	21	102	5	8	93	8	19	< 5	11	258	175	5	
Ba	1845	1068	1351	2397	1584	2070	2639	2153	1533	698	578	1271	1330	384	1672	2	
Sr	304	317	194	339	162	410	149	316	674	143	114	111	192	239	353	2	
Y	44	25	76	47	55	30	48	48	17	45	40	31	35	26	44	1	
Zr	567	99	659	653	452	400	1639	1132	245	757	340	1166	662	110	295	2	
Cr	< 20	< 20	< 20	< 20	< 20	< 20	< 20	< 20	60	< 20	< 20	< 20	< 20	100	30	20	
Co	7	10	4	8	7	18	2	3	15	1	3	2	3	32	21	1	
Ni	< 20	< 20	< 20	< 20	< 20	< 20	< 20	< 20	30	< 20	< 20	< 20	< 20	50	< 20	20	
Cu	< 10	30	< 10	10	40	20	10	10	20	< 10	< 10	< 10	10	< 10	40	10	
Zn	140	80	120	140	70	190	120	150	60	110	60	90	40	130	170	30	

(Continues)

TABLE 1 | (Continued)

ppm															
Ga	22	17	23	22	19	18	23	25	19	28	20	21	17	20	22	1
Ge	1	2	2	2	2	1	2	2	1	2	1	1	1	1	2	1
As	< 5	< 5	< 5	< 5	< 5	< 5	< 5	< 5	< 5	< 5	< 5	< 5	< 5	< 5	< 5	5
Rb	60	51	137	41	166	64	48	56	99	116	120	77	110	29	115	2
Nb	19	7	27	16	23	19	12	28	7	30	11	15	11	4	27	1
Mo	2	< 2	6	3	4	2	4	2	< 2	5	2	3	< 2	< 2	3	2
Ag	1.4	< 0.5	1.5	1.5	1	0.9	3.9	2.5	0.6	1.7	0.9	2.8	1.6	< 0.5	0.7	0.5
In	< 0.2	< 0.2	0.2	< 0.2	< 0.2	< 0.2	0.2	0.2	< 0.2	< 0.2	< 0.2	< 0.2	< 0.2	< 0.2	< 0.2	0.2
Sn	2	2	2	1	3	1	2	1	1	3	2	< 1	1	2	1	1
Sb	< 0.5	< 0.5	< 0.5	< 0.5	< 0.5	< 0.5	< 0.5	< 0.5	< 0.5	< 0.5	< 0.5	< 0.5	< 0.5	< 0.5	< 0.5	0.5
Cs	< 0.5	< 0.5	< 0.5	< 0.5	< 0.5	< 0.5	< 0.5	< 0.5	< 0.5	< 0.5	< 0.5	< 0.5	< 0.5	< 0.5	< 0.5	0.5
La	32.9	9.7	134	32.3	133	55.7	31.5	29.5	54.9	143	35.3	37.1	60.5	10.2	27.2	0.1
Ce	70.8	20.6	275	71.2	246	111	75.1	63.4	105	275	70.3	70.2	103	24.1	53.3	0.1
Pr	8.94	2.53	30.5	9.57	25.6	13.1	10.3	8.5	11.7	29.4	8.24	7.98	10.4	3.33	6.29	0.05
Nd	39.3	11.8	108	43	87.2	52.3	43.8	38.3	43.7	103	32.3	30.6	36.7	15.8	24.5	0.1
Sm	9	3.5	19.4	10.1	15.2	9.9	10.2	9.5	7.3	17.6	7.1	6.4	5.9	4.6	5.6	0.1
Eu	2.74	1.13	2.12	3.4	2.07	2.61	5.52	4.52	1.72	2.23	0.71	2.2	1.61	1.36	1.79	0.05
Gd	8.9	4.2	15.6	9.9	11.9	8.1	9.4	9.4	5.2	12.9	6.9	5.9	5.9	5	6.3	0.1
Tb	1.5	0.8	2.5	1.6	1.9	1.1	1.6	1.6	0.7	1.9	1.2	1	1	0.8	1.1	0.1
Dy	8.6	4.9	15.1	9.2	10.6	6.2	9	9.1	3.5	9.9	7.3	5.9	6.6	4.8	7.4	0.1
Ho	1.7	0.9	2.9	1.8	2.1	1.2	1.8	1.8	0.6	1.8	1.5	1.2	1.4	0.9	1.6	0.1
Er	4.8	2.6	8.2	5.1	6.1	3.1	5.3	5.2	1.7	4.9	4.4	3.7	3.8	2.6	4.7	0.1
Tm	0.67	0.35	1.15	0.7	0.84	0.46	0.82	0.79	0.25	0.63	0.64	0.55	0.58	0.37	0.74	0.05
Yb	4.4	2.2	7.5	4.6	5.4	2.8	5.7	5.6	1.6	4.1	4.2	4	4	2.3	5.3	0.1
Lu	0.73	0.32	1.11	0.73	0.83	0.43	0.94	0.92	0.23	0.68	0.67	0.69	0.66	0.35	0.84	0.01
Hf	13	3	15.1	14.9	11.3	8.8	26	22.7	6.1	17.7	9.4	25.4	16.2	3.1	8.7	0.2

(Continues)

TABLE 1 | (Continued)

ppm																
Ta	0.9	0.4	1.2	0.8	1.4	1.1	0.7	1.2	0.4	1.3	0.9	0.7	0.5	0.3	1.6	0.1
W	<1	<1	<1	<1	12	<1	<1	<1	<1	<1	<1	<1	<1	<1	<1	1
Tl	0.2	0.2	0.4	0.1	0.8	0.3	0.2	0.1	0.4	0.4	0.3	0.2	0.3	0.2	0.5	0.1
Pb	16	18	24	14	26	20	12	13	19	25	18	13	16	6	12	5
Bi	<0.4	<0.4	<0.4	<0.4	<0.4	<0.4	<0.4	<0.4	<0.4	<0.4	<0.4	<0.4	<0.4	<0.4	<0.4	0.4
Th	1.4	0.4	11.6	0.3	29.1	1.3	1.8	0.8	2.5	37.2	5.9	2.8	5.1	0.8	1.2	0.1
U	0.5	0.1	1.2	0.3	2.8	0.4	0.4	0.3	0.5	1.9	0.8	0.5	0.4	0.5	0.7	0.1

In the AFM magma classification diagram (Figure 5a) following Irvine and Baragar (1971), the source magma of CWCs exhibits a tholeiitic trend, while the majority of CHCs indicate a calc-alkaline trend. However, some CHCs (HC-2, HC-14, HC-15) display a geochemical signature consistent with a tholeiitic composition similar to that of the CWCs. In the majority of discrimination diagrams (which will be presented in subsequent sections), these samples (HC-2, HC-14, HC-15) share similar geochemical characteristics with the CWCs. Therefore, in geochemical diagrams, we have used the same triangular shape symbol to represent the CHCs but differentiated these samples with a different colour (green) to distinguish HC-2, HC-14 and HC-15.

In the $Na_2O + K_2O - CaO$ versus SiO_2 diagram, most CHCs represent calc-alkaline to alkali-calcic protolith signatures, whereas most CWC samples exhibit an alkali-calcic to alkalic signature (Figure 5b). The Total Alkali versus Silica (TAS) classification after Middlemost (1994) shows a wide distribution of bulk composition for both HC and WC, ranging from intermediate to felsic composition (Figure 5c). The protoliths of WC charnockites show limited variation in silica content with high total alkali compared to the HC, which has a majority of low total alkali content and a wide range of silica content. Therefore, the both calc-alkaline and tholeiitic CHCs are classified as andesitic to dacitic composition, while most CWCs are classified as trachydacite and trachyandesite (Figure 5c).

In the $(FeO_T/(FeO_T + MgO))$ versus SiO_2 diagram (Figure 5d), CWCs fall within the ferroan region. In contrast, the majority of both calc-alkaline and tholeiitic CHCs fall within the magnesian region (Figure 5d). The Aluminium Saturation Index (ASI) of the studied charnockites is less than 1 (ranging from 0.6 to 1 with an average of 0.9), with A/NK values over 1 (ranging from 1.1 to 1.9 with an average of 1.4), indicating a metaluminous signature (Figure 5e).

In the Harker diagrams, both the tholeiitic CHCs and CWCs of TiO_2, Fe_2O_3, CaO and MnO exhibit a negative correlation with SiO_2 (Figure 6a–d).

In the tholeiitic CHCs and CWCs, MgO content shows a consistent relationship with SiO_2, exhibiting minimal variation (Figure 6f). Both P_2O_5 and Al_2O_3 display a clear negative correlation with SiO_2 in these samples (Figure 6g,h). Similarly, Na_2O demonstrates a weakly defined negative correlation with SiO_2 in both tholeiitic CHCs and CWCs (Figure 6i). In contrast, the calc-alkaline CHCs reveal a distinct negative correlation specifically between FeO_T and SiO_2, as well as MgO and SiO_2.

4.2 | Rare Earth Elements (REEs)

The concentrations of rare earth elements (REEs) in charnockitic rocks are given in Table 1. The total REE contents of CHCs and CWCs are 65.5–548.7 ppm (average 210.5 ppm) and 177.4–623.0 ppm (average 312.1 ppm), respectively. In the chondrite-normalised diagram (Figure 7a), CWCs exhibit enrichment in Light REE (LREE) compared to Heavy REE (HREE). The tholeiitic and calc-alkaline CHCs, on the other hand, display

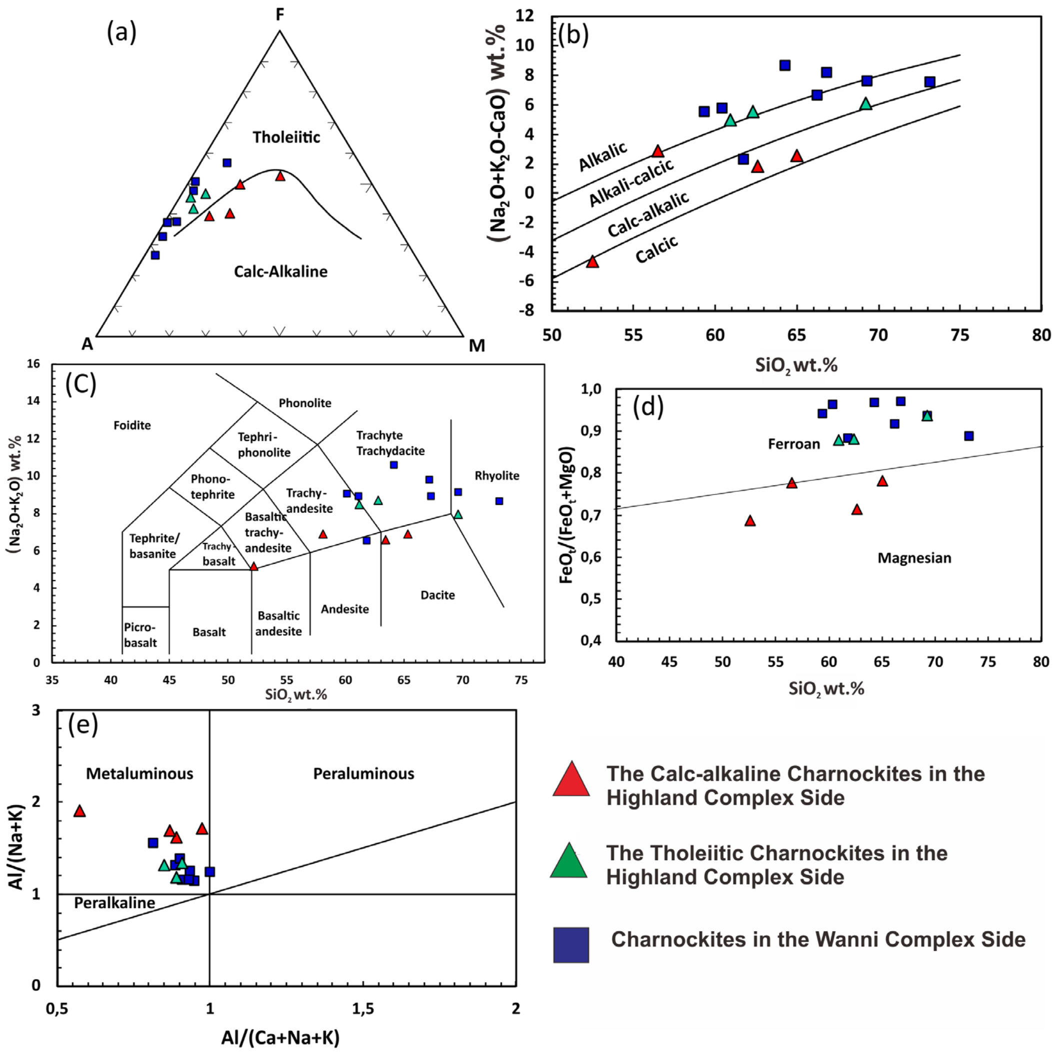

FIGURE 5 | (a) Alkali—FeO—MgO (AFM) diagram (after Irvine and Baragar 1971), (b, d) $Na_2O + K_2O$-CaO versus SiO_2 (after Frost et al. 2001) diagram for classification of HC and WC charnockites, (c) total alkali versus SiO_2 (TAS) diagram (after Middlemost 1994), (d) ($FeO^T/(FeO^T + MgO)$) versus SiO_2 (after Frost and Frost 2008), (e) A/NK versus A/CNK diagram (Shand 1948).

a relatively diverse nature. The tholeiitic samples show LREE enrichment and HREE depletion patterns similar to those observed in CWCs. However, in calc-alkaline samples, HC-3 and HC-31 exhibit a relatively flat REE pattern with minimal LREE fractionation, showing an almost identical HREE/chondrite ratio. Sample HC-32 also shows LREE enrichment compared to HREE, with a slight enrichment in middle to high REE as well. Most samples exhibit no significant Eu anomaly. One CHC (HC-15) and three CWCs (WC-8, WC-24 and WC-26) display a slight negative Eu anomaly. Two other CWCs (WC-19 and WC-20) show a positive Eu anomaly.

In the primitive mantle-normalised spider diagram (Figure 7b), CHCs exhibit negative anomalies for Th (except HC-15), Ta, Nb, Sr., P and Ti, along with positive anomalies for Ba, K and Pb. In contrast, CWCs show negative anomalies for Th (except WC-24), U, Ta, Nb, Sr., P and Ti with positive anomalies for Ba (only in samples WC-19 and WC-20), K, La, Pb and Zr (only in samples WC-19 and WC-27).

4.3 | Discrimination for the Nature of Protoliths and Tectonic Settings

In the SiO_2 versus Rb/Zr diagram after Harris, Pearce, and Tindle (1986) (Figure 8a), all charnockite samples fall within the I- and A-type granite fields in the granite classification discrimination diagrams of 10,000 × Ga/Al versus $Na_2O + K_2O$ (Figure 8b) and 10,000 × Ga/Al versus Zr (Figure 8c) (Whalen, Currie, and Chappell 1987), the protoliths of CWCs represent an A-type granite affinity, while the calk-alkaline CHCs fall within or margin of the other granite (I- and S-type granite) fields. Notably, three tholeiitic CHCs share chemical affinities with CWCs and fall into the A-type granite region.

A-type granitoids can be further divided into two chemical subgroups (A1 and A2) based on different sources and tectonic settings (Eby 1992). The A1 subtype is generally associated with continental rifts or intraplate non-orogenic environments, while the A2 subtype is mainly formed in post-collisional extensional

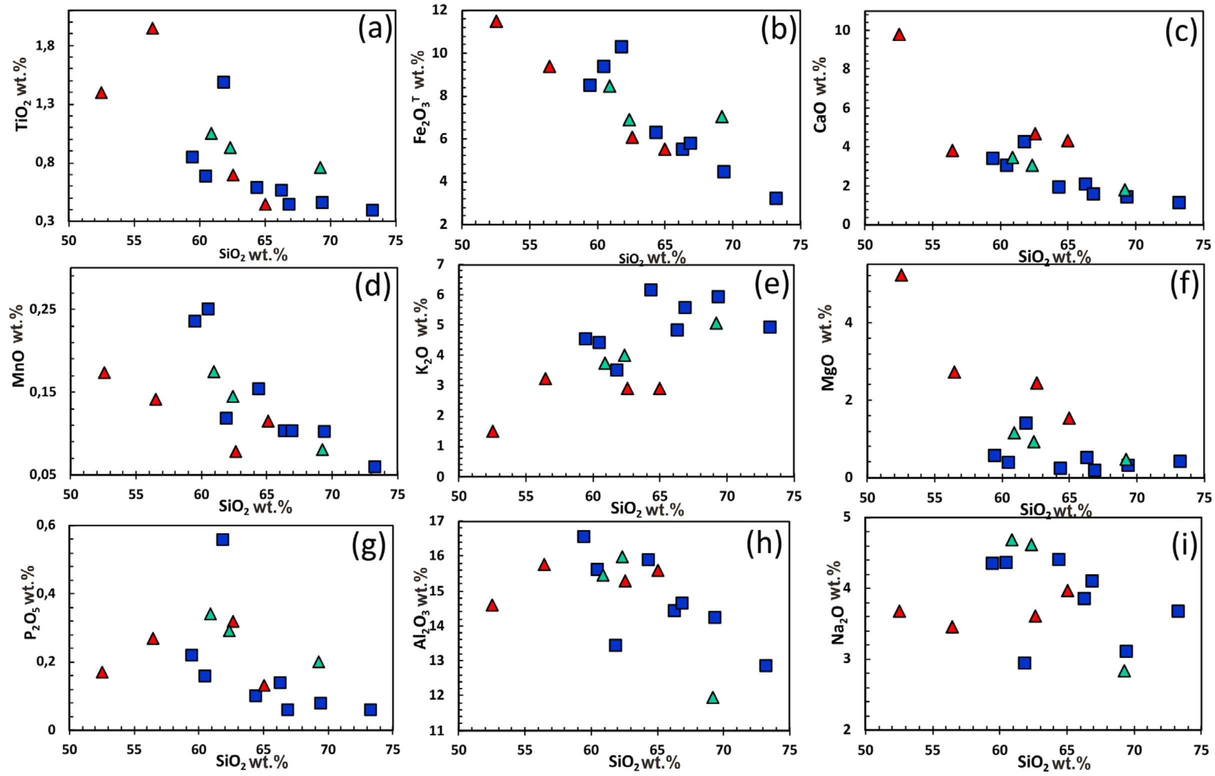

FIGURE 6 | Harker variation diagrams studied charnockites showing the variation in (a) TiO_2, (b) Fe_2O_{3T}, (c) CaO, (d) MnO, (e) K_2O, (f) MgO, (g) P_2O_5, (h) Al_2O_3, (i) Na_2O, as a function of the SiO_2 content.

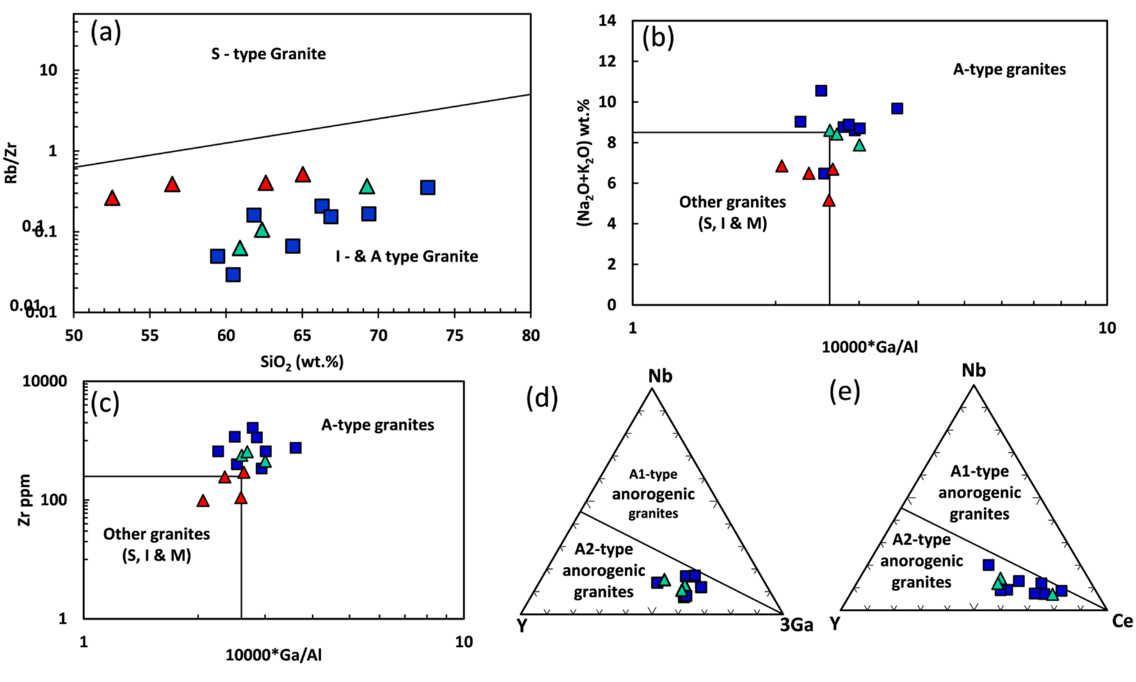

FIGURE 7 | (a) Chondrite-normalised REE patterns of studied samples from HC and WC; (McDonough and Sun 1995), (b) Primitive mantle-normalised trace elements Spider diagrams (Sun and McDonough 1989).

environments (Eby 1990, Eby 1992). Protoliths with an A-type granite signature were further classified using the Nb-Y-Ce and Nb-Y-3Ga diagrams (Figure 8d,e). All samples fall within the A2 subtype region.

In the Nb versus Y and Nb + Y versus Rb diagrams (after Pearce, Harris, and Tindle 1984) (Figure 9a,b), CWCs consistently fall within the Within Plate Granite field or close to the Within-Plate Granite in the Volcanic Arc Granite margin. The tholeiitic

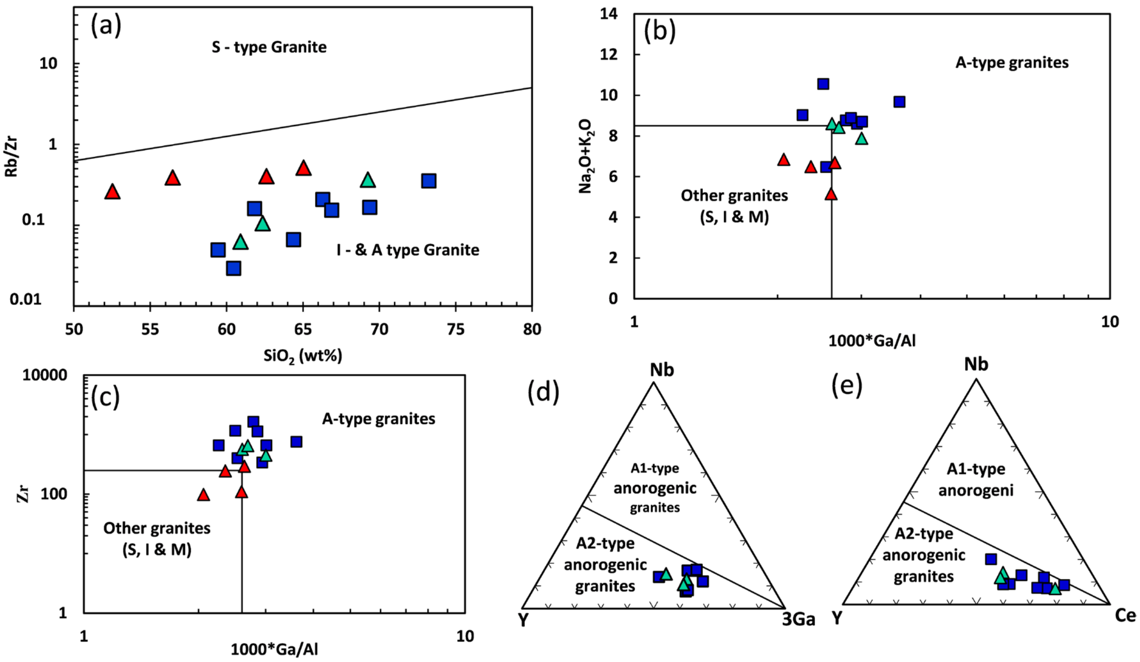

FIGURE 8 | (a) Rb/Zr versus SiO_2 (after Harris, Pearce, and Tindle 1986) (b) 10,000 × Ga/Al versus $K_2O + Na_2O$ (c) 10,000 × Ga/Al versus Zr (c) and (d) after Whalen, Currie, and Chappell (1987), (e) ternary Nb–Y–Ce (f) ternary Nb–Y–3Ga. (e) and (f) after Eby (1992).

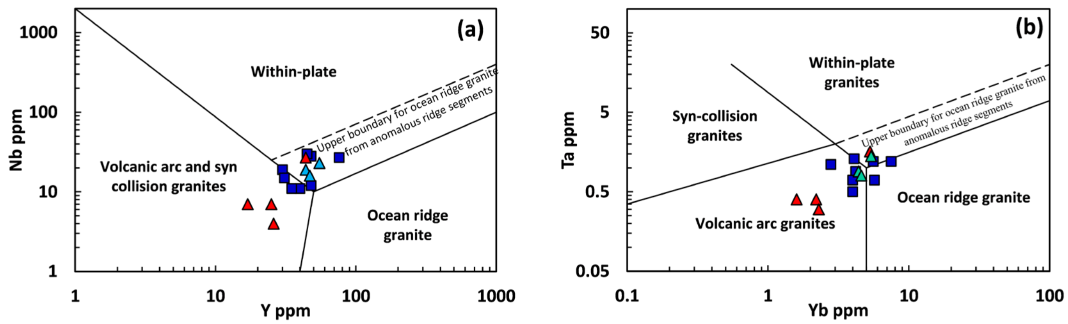

FIGURE 9 | Discrimination diagrams for HC and WC Charnockitic samples. (a) Y versus Nb diagram; (b) Y + Nb versus Rb diagram (a and b after Pearce, Harris, and Tindle (1984)).

CHCs also exhibit signatures of within-plate granite, similar to CWCs.

5 | Geochronology

Zircon U–Pb dating for selected samples was conducted at the State Key Laboratory of Lithospheric Evolution, Institute of Geology and Geophysics, Chinese Academy of Sciences (IGGCAS), Beijing, China. We utilised the laser ablation-split-stream inductively coupled plasma-mass spectrometry (LA-SS-ICP-MS) technique for zircon U–Pb dating and trace element analysis on three samples of CWCs (WC-19, WC-27 and WC-28) and one sample of CHCs (HC-2). The LA-SS-ICP-MS setup includes an UP-193 Solid-State laser (193 nm, New Wave Research Inc.) coupled with a quadrupole ICP-MS (Agilent 7500a).

For most analyses, a laser spot size of 40 μm was used, though smaller spot sizes were employed for small grains or thin zircon rims. The counting times were 15 ms for ^{204}Pb, ^{206}Pb, ^{207}Pb and ^{208}Pb, 10 ms for ^{238}U, ^{235}U and ^{232}Th. NIST610 glass was utilised as the external standard, and ^{28}Si was used as the internal standard for calibrating zircon analyses. The zircon standard 91,500 was employed for correcting U–Pb isotope fractionation effects (Wiedenbeck 1995). Additionally, zircon standard GJ-1 (613 ± 6 Ma) (Elhlou et al. 2006; Jackson et al. 2004; Xie et al. 2008) was used as a secondary standard to monitor age measurement deviations. The apparent $^{208}Pb/^{238}U$ dates for GJ-1 ranged from 605 to 618 Ma, consistent with the recommended value of 613 Ma (Elhlou et al. 2006; Jackson et al. 2004; Xie et al. 2008). Error correlation was considered as 0.7 (Andersen et al. 2019), and common lead correction followed the method of Andersen (2002). Detailed descriptions of the laboratory, instruments and analytical procedures can be found in Xie et al. (2008).

The results of the U–Pb zircon geochronological analysis for samples WC-27, WC-19, WC-28 and HC-2 are presented in Tables S2–S5. The cathodoluminescence images of the analysed zircons from these samples are shown in Figure 10a–d. The

Concordia plots for these samples are displayed in Figure 11a–d. Uncertainties in each analysis were described at the two-sigma level.

5.1 | WC-27

The zircon grains from this sample predominantly exhibit an elongated shape, as depicted in the cathodoluminescence (CL) images shown in Figure 10a. A few grains display irregular and rounded shapes. The zircon grains are generally subhedral to anhedral, with sizes ranging from 100 to 250 μm and length-to-width ratios varying approximately between 1:1 and 3:1. These grains are transparent to translucent and colourless, with some showing tiny needle-like and copper-brown rounded inclusions.

In the CL images, most zircon grains exhibit oscillatory zoning, characterised bright sector zoned core and dark unzoned rim. Some grains also display sector and patchy zonation patterns (Figure 10a). Out of 26 analysed spots, 23 were used to construct the Concordia plot (Figure 11a) and had acceptable discordance values (Table S2). Among these, one zircon having a dark unzoned rim yielded a late Neoproterozoic $^{206}Pb/^{208}U$ age of 562 ± 4 Ma (Figure 11a). The remaining zircon spots in mainly core and mantle areas of the grains produced ages ranging from 801.6 ± 11.47 Ma to 995.6 ± 20.42 Ma. The sample produced lower and upper intercept ages of 576 ± 37 Ma and 1011 ± 46 Ma, respectively (MSWD = 0.98).

The zircon with a rim age of 562 ± 4 Ma has Th and U contents of 38 and 1185 ppm, respectively, and a Th/U ratio of 0.03. In contrast, the Th and U contents, as well as the Th/U ratios of the other selected zircons, range from 16 to 292 ppm, 32 to 478.15 ppm and 0.40 to 0.78 ppm, respectively (Table S2).

5.2 | WC-19

Angular-shaped, anhedral zircon grains are predominant in this sample, with a few rounded and elongated grains also present. The lengths of the grains range from 100 to 200 μm, and the length-to-width ratios vary between 1:1 and 2:1. The zircons are translucent to transparent, with some grains displaying iron leach patches. Most grains exhibit core-rim zonation, characterised by a dark rim and a light core texture, while a few grains

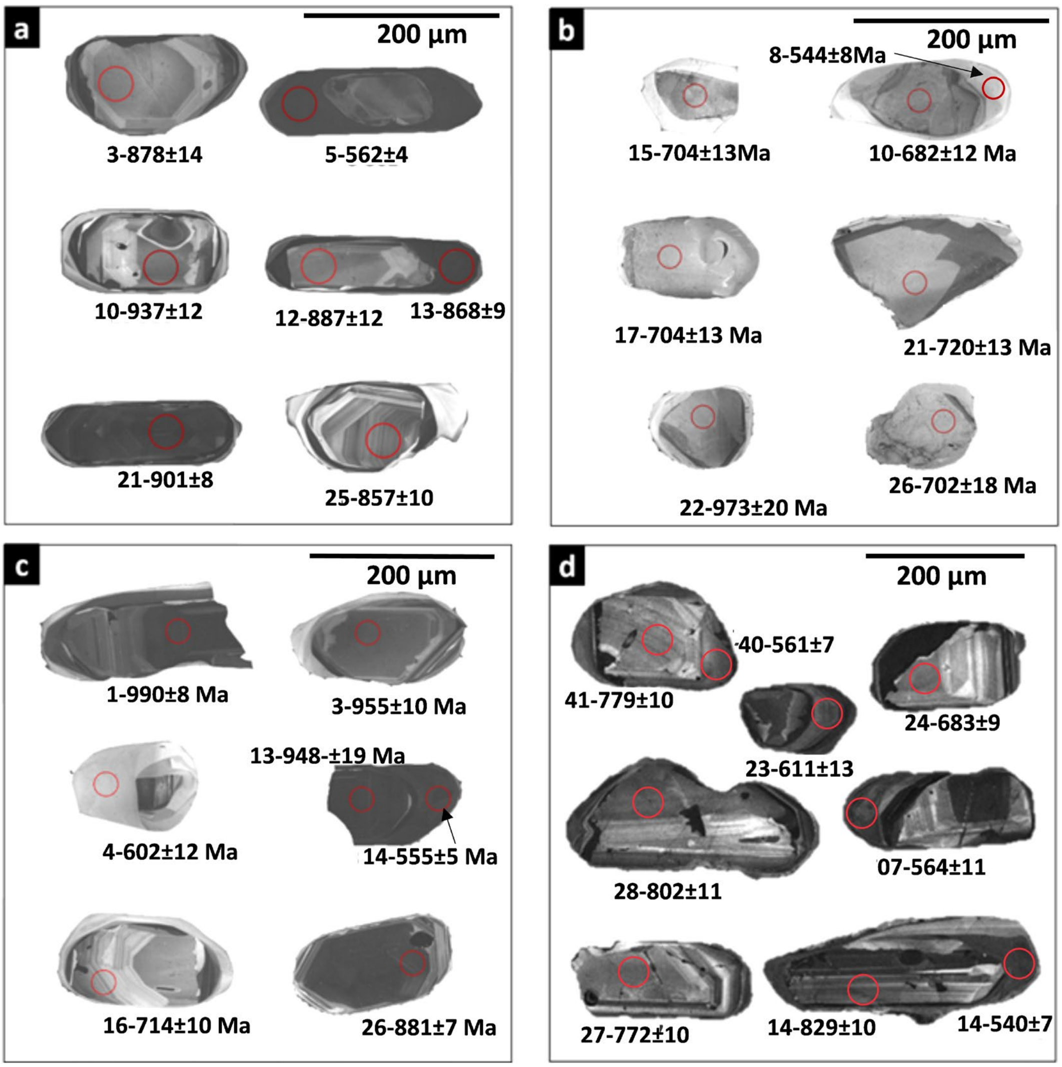

FIGURE 10 | Cathodoluminescence images of representative zircon grains from samples (a) WC-27, (b) WC-19, (c) WC-28 and (d) HC-2.

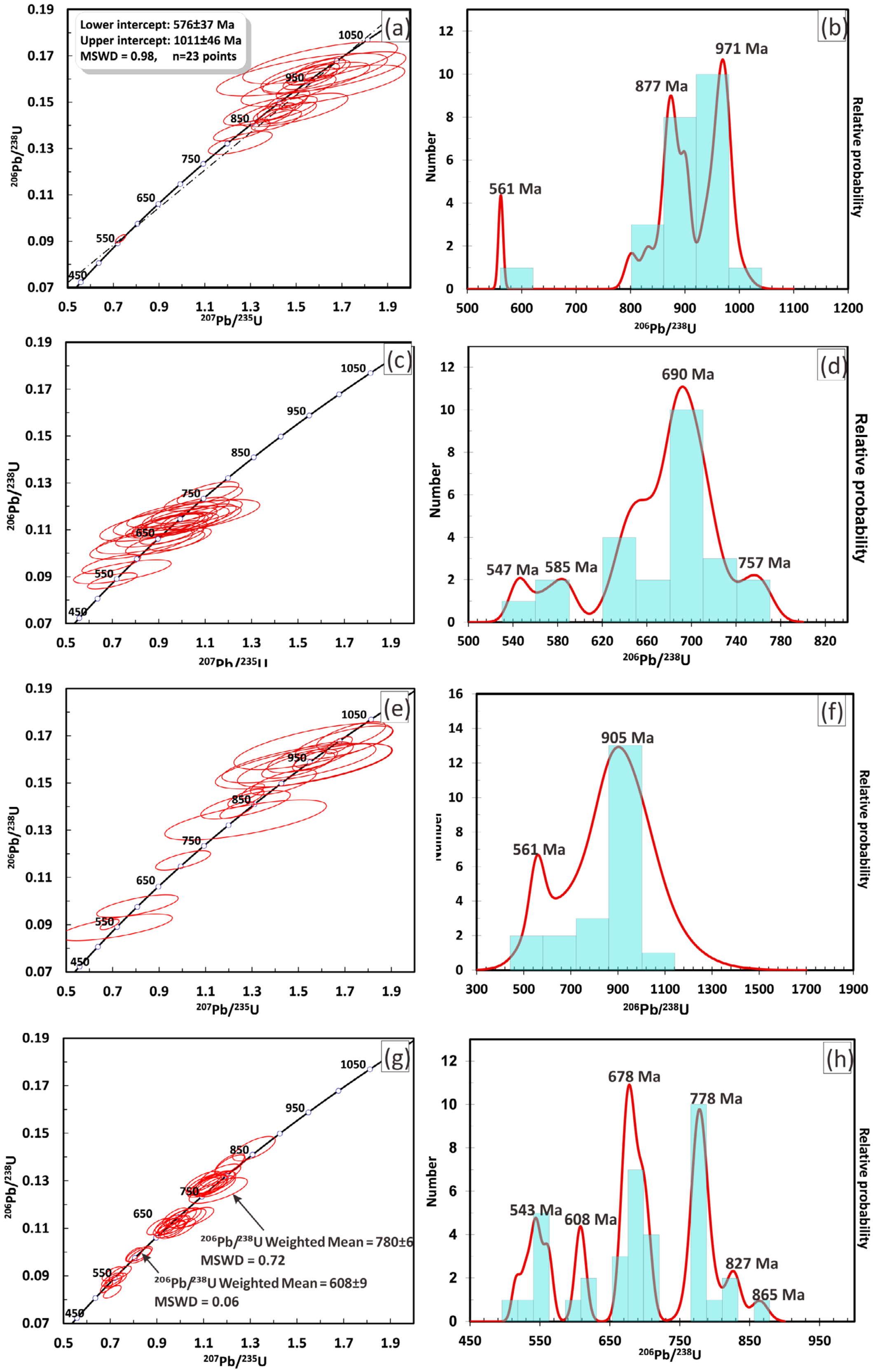

FIGURE 11 | Concordia diagrams showing weighted mean $^{206}Pb/^{238}U$ age of zircons age data histograms and probability density plots of (a) WC-27, (b) WC-19, (c) WC-28 and (d) HC-2.

show dark cores with bright rims. The core areas of some grains show sector and occasionally oscillatory zonation, as illustrated in the CL images (Figure 10b).

Out of the 28 zircon spots analysed, 24 were used to plot the Concordia diagram (Figure 11b). The distribution of $^{206}Pb/^{238}U$ dates spans a wide range from 544 ± 8 Ma to 763 ± 11 Ma and shows clustering into two distinct groups on the Concordia diagram. No meaningful lower and upper intercept ages were determined for this samples. The histograms show $^{206}Pb/^{238}U$ age peaks at approximately 547 and 585 Ma, which correspond to zircons with light rims, and at 690 Ma and 757 Ma, which correspond to zircons cores. The zircon ages at peak values of 547 and 585 Ma have Th/U ratios ranging from 0.31 to 0.39 (see Table S3). In contrast, the zircon ages at peak values of 690 and 757 Ma display Th/U ratios ranging from 0.14 to 0.57, respectively (see Table S3).

5.3 | WC-28

The zircons obtained from this sample predominantly exhibit elongated shapes, with a smaller number of rounded grains. They are mostly subhedral to anhedral, ranging in length from 100 to 300 μm, with length-to-width ratios varying from 1:1 to 4:1. The zircons are transparent to translucent and colourless, sometimes containing tiny needle-shaped inclusions. CL images (Figure 10c) reveal fine oscillatory zonings, characterised by a uniform dark core that gradually fades to a grey colour toward the rim. Out of a total of 29 zircon spots analysed, 21 were used to determine the geochronology for this sample.

The histograms show two $^{206}Pb/^{238}U$ date peaks at ca. 561 and 905 Ma. The first peak primarily corresponds to dates from zircon rims, while the latter is mainly associated with zircon cores and mantles. Zircon dates at the peak value of 561 Ma exhibit Th/U ratios ranging from 0.17 to 1.12 (see Table S4). In contrast, zircon dates at the peak value of 905 Ma display Th/U ratios ranging from 0.22 to 0.74 (see Table S3).

5.4 | HC-2

Most of the zircon grains from this sample display elongated and euhedral shapes. The zircons range in length from 200 to 600 μm, with length-to-width ratios varying from 1.1 to 4:1. CL images (Figure 10d). Some of the zircon grains exhibit dark cores and grey mantles with oscillatory zoning in the mantle areas. Some other zircon cores exhibit sector zonation (Figure 10d), and the light-coloured rim areas suggest metamorphic overgrowth (Figure 10d).

Zircon date clusters are clearly identifiable on the Concordia diagram. Weighted mean $^{206}Pb/^{238}U$ zircon ages were calculated separately for these clusters, with an MSWD <1 obtained for only two clusters (Figure 11g). These clusters yielded weighted mean $^{206}Pb/^{238}U$ ages of 780 ± 6 Ma (MSWD = 0.72; $n = 11$, data points HC-2-10, −11, −13, −17, −22, −27, −28, −31, −33, −34 and −41 in Table S5), and 608 ± 9 Ma (MSWD = 0.06; $n = 3$, data points HC-2-23, −26, and −44 in Table S5), respectively (Figure 11g). The first date cluster is primarily derived from zircon cores and mantles, whereas the latter two clusters are from zircon rims. The Th/U ratios of zircons in these clusters range from 0.03 to 0.6 and 0.09 to 0.12, respectively. In the histograms, age peaks are identified at approximately 543, 608, 678, 778, 827 and 865 Ma.

6 | Discussion

6.1 | Tectonic Insights of Protoliths of Charnockites Across the Northeastern HC-WC Boundary

Due to the closely interleaved nature of charnockites with metasedimentary lithologies, some early workers considered the charnockitic rocks in the Highland Complex of Sri Lanka as metasediments (e.g., Vitanage 1959; Cooray 1962). However, later geochemical studies (e.g., Wickremasinghe 1969; Jayawardena and Carswell 1976; Munasinghe and Dissanayake 1980; Pohl and Emmermann 1991; Santosh et al. 2014; He et al. 2016; Abewardana et al. 2023) have shown that the compositions and various geochemical trends of charnockitic rocks in the Sri Lankan basement are comparable to those of igneous rocks. Geochemical signatures of granitoids often reflect different tectonic settings during orogeny, including subduction, syn- to post-collisional and post-orogenic extensional settings (e.g., Chappell and White 1974, 1992; Brown 1994; Barbarin 1999; Bonin 2007; Wang et al. 2018). This section explores the origin of the source magmas for the protoliths of the studied charnockites and provides insights into the tectonic settings where these protoliths were emplaced, as well as their relationship to global tectonic cycles.

The upper and lower intercept ages of 1011 and 576 Ma for Sample WC-27 from the CWCs represent the crystallisation and metamorphic ages, respectively (Figure 11a). These ages align well with the protolith ages of metaigneous rocks reported in previous studies (e.g., Hölzl et al. 1994; Kröner, Kehelpannala, and Hegner 2003; Santosh et al. 2014). Similarly, in Sample WC-28, zircon cores and mantles with sector and occasional oscillatory zoning yield $^{206}Pb/^{238}U$ age peaks at approximately 905 Ma, which represent the crystallisation age. The zircon rims, with $^{206}Pb/^{238}U$ age peaks at 561 Ma, represent the metamorphic age. This Early to Middle Neoproterozoic magmatism correlates with the global processes associated with the formation and breakup of the Rodinia supercontinent (e.g., Meert and Torsvik 2003; Li et al. 2008). Reconstruction models suggest that Rodinia was assembled through widespread orogenic events between 1300 and 900 Ma, involving nearly all continental blocks known at that time (e.g., Jacobs et al. 2008; Johansson 2009; Roberts and Slagstad 2015; Martin et al. 2020).

Sample WC-19 from the CWCs shows $^{206}Pb/^{238}U$ age peaks at approximately 547 and 585 Ma (Figure 11c,d), which correspond to zircons with overgrowth light rims representing metamorphic ages. Additionally, an age peak around 757 Ma corresponds to zircon cores, likely representing the crystallisation age. The zircon core and mantle age peak around 690 Ma may reflect resetting of protolith zircon during metamorphism or the formation of new zircon during a tectonothermal event after the crystallisation of the protolith. Similarly, in Sample HC-2, zircon cores and mantles with sector and oscillatory zoning yield a weighted mean $^{206}Pb/^{238}U$ age of 780 ± 6 Ma (MSWD = 0.72; $n = 11$), which can be interpreted as the most plausible crystallisation age (Figure 11g,h). A histogram peak at 678 Ma may indicate the resetting of protolith zircon during metamorphism or the formation of new zircon during a tectonothermal event.

The zircon rim ages are represented by $^{206}Pb/^{238}U$ date clusters of 608 ± 9 Ma (MSWD = 0.06) and histogram peak ages ca. 543 Ma represent metamorphic ages (Figure 11g,h). The dispersal of Rodinia was driven by widespread continental rifting between approximately 825 and 740 Ma (e.g., Li et al. 2008; Martin et al. 2020). The Late Mesoproterozoic (1100–900 Ma) and Middle Neoproterozoic (800–750 Ma) crystallisation ages of protoliths from metaigneous rocks observed in this and previous studies indicate a connection between the CWCs and the formation and breakup of the Rodinia supercontinent (e.g., Hölzl et al. 1994; Kehelpannala 2004; Kröner, Kehelpannala, and Hegner 2003; Santosh et al. 2014).

The later Neoproterozoic ages, ranging from 610 to 540 Ma, represent metamorphism of Sri Lankan basement rocks, which occurred concurrently with the amalgamation of the Gondwana supercontinent, as interpreted by several previous researchers (e.g., Hölzl et al. 1994; Santosh et al. 2014; Dharmapriya et al. 2015; He et al. 2016; Kitano et al. 2018).

Previous studies indicate that zircon crystallised from granitic magma typically exhibits a high Th/U ratio (usually > 0.1), whereas zircon formed through metamorphic processes generally has a low Th/U ratio (usually < 0.1) (e.g., Rubatto and Hermann 2003; Whitehouse, Kamber, and Moorbath 1999). However, in the zircons analysed in this study, the Th/U ratios of overgrowth zircon rims also show high values (> 0.1). This variation can be attributed to metamorphic processes such as overgrowth on igneous cores, partial melting, metasomatism and fluid interactions during high-grade metamorphism. High-temperature rocks often display Th/U ratios > 0.1 (Harley and Kelly 2007; Rubatto 2017; Yakymchuk, Kirkland, and Clark 2018).

Although HC-2 shows Middle Neoproterozoic crystallisation ages around 780 Ma (Figure 11d), similar to CWCs, the classification of the sample as a WC charnockite cannot rely solely on U–Pb geochronology. Recent advancements in U–Pb zircon geochronology indicate evidence for at least four magmatic episodes in the HC. Metaigneous rocks, including charnockites, predominantly yield middle to late Paleoproterozoic crystallisation ages around 1950–1800 Ma (Kröner and Williams 1993; Hölzl et al. 1994; Santosh et al. 2014; Kitano et al. 2018). Zhao et al. (2023) noted the emplacement of some charnockitic protoliths in the HC during the Neoarchaean to early Paleoproterozoic around 2500–2450 Ma. Additionally, Middle Neoproterozoic ages (850–670 Ma; Hölzl et al. 1994; Kitano et al. 2018) and rare Late Neoproterozoic crystallisation ages (580 Ma) have also been reported (He et al. 2016).

To differentiate between WC and HC charnockites, one approach is to consider crust formation ages such as εHf(t) values of zircon. For instance, He et al. (2016) reported negative εHf(t) values ranging from −6.7 to −12.6 with crustal residence ages (TCDM) of 2039–2306 Ma for HC charnockite, suggesting magma derivation through melting of a Paleoproterozoic source. In contrast, charnockites from the Wanni Complex (collected near Kurunegala, Figure 1a) exhibit clearly positive εHf(t) values up to 13.1 and TCDM ages in the range of 937–1458 Ma, indicating a much younger and depleted mantle source. In the absence of crust formation ages, geochemical characteristics offer an alternative solution due to the contrasting geochemical signatures of HC and WC metaigneous rocks.

Considering the geochemical signatures of charnockites in this study, the protolith magma of the studied CWCs shows a tholeiitic affinity (Figure 5a). Unlike calc-alkaline magma, tholeiitic magmatism can occur in diverse tectonic settings such as mid-oceanic ridges, continental rift zones, volcanic island arcs, back-arc basins and oceanic plateaus (e.g., Sen and Stern 2021; Zimmer et al. 2010; Chin 2018). The early type is primarily associated with subduction-related magmatism (e.g., Sen and Stern 2021; Chin 2018). Meantime all charnockite samples fall within the I- and A-type granite fields in the SiO_2 versus Rb/Zr diagram after Harris, Pearce, and Tindle (1986) (Figure 8a), indicating that the protoliths of the studied charnockites are not products of melting of precursor or sedimentary rocks (Chappell and White 1974). S-type granites are typically peraluminous and contain high K_2O wt.% and Rb/Zr ratios. The metaluminous signature of all the charnockites supports this discrimination, and moderate K_2O wt.% along with relatively low Rb/Sr ratios further confirms that none of the protoliths of the studied charnockites exhibit an S-type granite signature. These protoliths of CWCs are classified as Fe-rich (Figure 5d), metaluminous (Figure 5e), A-type granites (Figure 8b,c). Although samples HC-2, HC-14 and HC-15 were collected from the HC side, they share the geochemical signatures of CWCs.

Frost and Frost (2008) interpreted that many of these ferroan charnockites are isotopically primitive, suggesting they have been derived largely or entirely from the differentiation or melting of tholeiitic melts. Metaluminous granites are formed through partial melting of mafic to intermediate source rocks, fractional crystallisation and magma mixing processes in various tectonic settings, including convergent boundaries, post-collisional regions and intraplate environments (e.g., King et al. 1997; Klimm et al. 2003; Shellnutt and Zhou 2007; Wang et al. 2013). A-type granites are known to signify extensional environments in various tectonic settings, including within-plate, post-collisional, or back-arc environments (e.g., Loiselle and Wones 1979; Eby 1992; Bonin 2007; Condie et al. 2023). Pohl and Emmermann (1991) also pointed out that the granitic and syenitic gneisses of the WC show typical chemical characteristics of A-type affinity. According to Eby (1992), A1- and A2-type granites originate from different sources and form in distinct tectonic settings: A1-type granites are typically associated with anorogenic settings such as hotspots, plumes, or continental rift zones, while A2-type granites are typically found in post-collisional settings or similar environments (e.g., Jiang et al. 2020). All the above-mentioned samples were classified as A2 subtype (Figure 8d,e). In tectonic discrimination diagrams, most of these sample's plot within the within-plate granite field (Figure 9a,b). In the chondrite-normalised diagram (Figure 7a), except for WC-28, all other samples show high to moderate enrichment in LREE and little fractionation of HREE. The negative Eu anomalies of samples WC-8, WC-24 and WC-26, and HC-15 suggest plagioclase fractionation (Shearer and Papike 1989; Rudnick 1992; He et al. 2016). In contrast, the positive Eu anomalies in samples WC-19 and WC-20 likely indicate the presence of residual feldspar in their protoliths samples (e.g., Rudnick 1992), as supported by the relatively high modelled percentage of plagioclase. The Harker diagrams coupled with the mineralogy provide compelling evidence for the fractional crystallisation of the protoliths in the studied tholeiitic CHCs and CWCS (tholeiitic charnockites), as indicated by the systematic removal of TiO_2-, FeO-, CaO- and MnO-bearing minerals, coupled with late-stage enrichment of K_2O in potassium-rich minerals (Figure 6a–e). This observation suggests that TiO_2-, FeO-, CaO- and MnO-bearing minerals were extracted from the residual magma during fractional crystallisation (e.g., Li et al. 2011). Based on the mineralogy of the studied tholeiitic charnockites, TiO_2 is predominantly associated with ilmenite; FeO occurs in two pyroxenes, hornblende and ilmenite; CaO is present in plagioclase, clinopyroxene and hornblende; and MnO is primarily found in orthopyroxene, clinopyroxene and occasionally in ilmenite (Jayathilake et al. 2023). The negative trends of TiO_2, FeO, CaO and MnO observed in the Harker diagrams reflect the fractionation of ilmenite, pyroxenes, plagioclase and hornblende from the residual melt. Additionally, the enrichment of K_2O with increasing SiO_2 indicates the late-stage crystallisation of potassium-rich minerals, such as alkali feldspar and micas, during magma cooling and differentiation (e.g., Forni et al. 2018).

The negative correlation of MgO with SiO_2 in calc-alkaline charnockites (CHCs), coupled with the relatively homogeneous MgO content in CWCs (charnockite variants) and tholeiitic CHCs, suggests that MgO fractionation occurred at an earlier stage in the protoliths of calc-alkaline CHCs compared to the tholeiitic charnockites. The negative correlation of P_2O_5 with SiO_2 (Figure 6g) is consistent with the fractionation of apatite, an accessory mineral in the protoliths of studied tholeiitic charnockites (e.g., Busa, Clochiatti, and Cristofolini 2002). Similarly, the negative correlation of Al_2O_3 with SiO_2 (Figure 6h) highlights the fractionation of alkali feldspar, biotite and hornblende in protoliths of tholeiitic charnockites.

The poorly defined negative correlation of Na_2O with SiO_2 in both tholeiitic CHCs and CWCs (Figure 6i) suggests the incorporation of Na_2O into plagioclase feldspar during fractional crystallisation. These distinct geochemical trends, combined with mineralogical observations, confirm that the magma underwent progressive differentiation and crystallisation processes of tholeiitic CHCs and majority of CWCs. This is in contrast to magma mixing or crustal assimilation, which would result in scattered data points rather than the well-defined trends observed in the Harker diagrams (e.g., Harker 1909; Ahankoub et al. 2013; Zhang and Audétat 2017).

Combining the above geochemical signatures, such as the Fe-rich, metaluminous A2-type protoliths of the CWCs and samples the tholeiitic CHCs, suggests that they originated from fractionated tholeiitic-type magmas in post-collisional or post-orogenic extensional tectonic settings within a continental environment. The calc-alkaline CHC samples HC-3 and HC-21 exhibit similar behaviour, grouping together, while HC-31 and HC-32 show distinct patterns, representing different trends in most Harker diagrams (Figure 6a,c–e,g–i). These contrasting trends may reflect variations in processes such as magma mixing or crustal assimilation. Calc-alkaline rocks are typically associated with subduction zones, where fluids released from the subducting slab interact with the mantle wedge and the overlying crust, resulting in the mixing of diverse magma sources and crustal assimilation (Kelley and Cottrell 2009; Vermeesch and Pease 2021).

Based on whole-rock major and trace element analyse and U–Pb zircon geochronology, Kröner, Kehelpannala, and Hegner (2003) interpreted that the large volumes of 1100–880 Ma calc-alkaline granitoid rocks in the WC of Sri Lanka likely indicate these domains were produced in active margin settings, probably as Grenville-age magmatic arcs attached to the Rodinia supercontinent. Their sampling localities were in the central and north-central parts of the WC. Recently, Abewardana et al. (2023) also studied the wholerock major element signatures of the WC charnockite. Their samples, collected from central to north-central parts of the WC, also exhibit calc-alkaline signatures of parent magma, similar to the observations of Kröner, Kehelpannala, and Hegner (2003). However, a sample collected close to the northern margin of the Complex (sample SL/CM/20) showed characteristics of tholeiitic-type magma, aligning with the results of this study. These findings suggest that the protoliths of charnockites in the northern to northeastern parts of the WC experienced a distinct evolutionary history compared to those in the central and north-central regions of the Complex. Previous studies (e.g., Pohl and Emmermann 1991; Kröner, Kehelpannala, and Hegner 2003; Abewardana et al. 2023) focusing mainly on the central and north-central parts of the Complex, interpreted the WC as a continental arc produced from subduction-related magmatism. However, the Fe-rich metaluminous, A2-type granitic signatures with tholeiitic-type affinity found in the studied CWCs indicate that the protoliths of these charnockites originated from fractionation in extensional tectonic settings within a continental environment in the Rodinia supercontinent. In contrast, protoliths of calc alkaline CHCs (samples HC-3, HC-21, HC-31 and HC-32) were classified as Mg-rich metaluminous I-type granites. Samples HC-3 and HC-31 show a nearly flat REE pattern, indicating little or no fractionation of the middle relative to the heavy REE (samples HC-3 and HC-31) consistent with melting of a source under the absence of garnet (e.g., Manikyamba et al. 2014). However, HC-21 shows high fractionation of LREE compared to HREE. In tectonic discrimination diagrams, except HC-21, the rest of the three samples plot in the volcanic arc granite field, suggesting that the protoliths of those rocks were derived from arc-related magmas. The geochemical signatures of these four samples indicate that their protoliths were derived from subduction-related volcanic arc magmatism.

In most recent Gondwana reconstruction models, the western extension of the HC and WC of Sri Lanka is correlated with the Trivandrum Block and Southern Madurai Block of the Southern Granulite Terrain in India (e.g., Kröner, Santosh, and Wong 2012; Dharmapriya et al. 2016; Ratheesh-Kumar et al. 2020). These correlations among the terrains were established based on petrological, geochronological, geochemical and geophysical studies (e.g., Kröner, Santosh, and Wong 2012; Dharmapriya et al. 2016; Santosh et al. 2017; Ratheesh-Kumar et al. 2020). Historically, the eastern extension of the HC and WC has been correlated with East Antarctica (e.g., Shiraishi et al. 1994; Dunkley et al. 2014, 2020). Since our present study is primarily focused on the northeastern part of the HC and WC, we aim to explore the potential correlation of these two complexes with East Antarctica.

The Lützow–Holm Complex in East Antarctica is traditionally classified into the Skallen Group, Ongul Group and Okuiwa Group based on lithostratigraphy (Yoshida 1978, 1979). The Skallen Group is primarily defined by Archean to Paleoproterozoic zircon ages, while the Ongul and Okuiwa Groups are characterised by Mesoproterozoic to Neoproterozoic zircon ages (Shiraishi et al. 1994, 2003; Dunkley et al. 2014; Tsunogae et al. 2014; Tsunogae, Yang, and Santosh 2015, 2016). Previous researchers, including Dunkley et al. (2014), Osanai et al. (2016) and Kitano et al. (2018), found similarities between the HC and WC of Sri Lanka and the Skallen, Ongul and Okuiwa Groups, respectively. Recent advancements in geochronology have reclassified the Lützow-Holm Complex into the Innhovde Suite, Rundvågshetta Suite, Skallevikshalsen Suite, Langhovde Suite, East Ongul Suite and Akarui Suite, from southwest to northeast (Dunkley et al. 2020). The Langhovde Suite (LHV) consists of metaigneous protoliths dated between 1100 and 1050 Ma, which are comparable to the WC protolith ages. The HC correlates with the Rundvågshetta Suite and Skallevikshalsen Suite, which have been divided based on the presence of Neo-Archean to early Proterozoic protoliths in the Rundvågshetta Suite and middle Proterozoic protoliths (2100–1800 Ma) in the Skallevikshalsen Suite (Dunkley et al. 2020). Recent geochronological advancements in the HC indicate the incorporation of early Proterozoic protoliths (ca. 2460 Ma, Zhao et al. 2023) alongside predominantly middle Proterozoic protoliths (1800–1900 Ma). Geochemical studies of mafic granulite from Langhovde suggest a subduction-related volcanic arc or within-plate affinity (Tsunogae, Yang, and Santosh 2016), similar to the WC rocks in the present study. Takahashi et al. (2018) reported that the geochemical characteristics of most felsic to mafic meta-igneous rocks from the Austhovde and Telen areas, which belong to the Rundvågshetta Suite and Skallevikshalsen Suite, exhibit a volcanic-arc affinity similar to the calc-alkaline CHCs described in this study. Additionally, the authors inferred that the protoliths of two mafic granulites from Austhovde represent non-volcanic-arc basalts, such as E-MORB, suggesting the accretion of oceanic lithosphere along with volcanic-arc components during subduction–collision events, akin to those interpreted for the HC by Santosh et al. (2014).

The obtained geochemical and geochronological results, along with sampling localities concerning the inferred northeastern part of the HC–WC boundary, support the hypothesis that the tholeiitic charnockites, collected from the HC side relative to the current inferred tectonic boundary, should be considered part of the WC. As illustrated in Figure 1b, HC-3, an I-type granite with an Mg-rich, calc-alkaline signature, is located near the present inferred HC-WC tectonic boundary, whereas HC-2, HC-14 and HC-15 are situated further toward the HC from this boundary. This distribution may reflect the nature of the contact between the northeastern parts of the two complexes around Trincomalee, where the WC is thrusted on top of the HC. Erosion of the exposed crustal section has led to the local distribution of WC rock remnants approximately 10–15 km toward the HC from the suggested Nd modal age boundary (Kröner, Cooray, and Vitanage 1991; Kröner et al. 1991). This creates a mixed rock zone that is composed of a scattering of HC and WC rocks. Field investigations have identified marble bands (see Satish-Kumar et al. 2021), a lithology characteristic of the HC, in the northern part of Trincomalee town (Figure 1b) further northward from tholeiitic CHCs HC-15, providing further evidence for this interpretation (). Field investigations have further identified marble bands—a lithology characteristic of the HC—in the northern part of Trincomalee town (see Satish-Kumar et al. 2021), located farther north of the tholeiitic charnockites, including HC-15 (Figure 1b). This observation provides additional evidence supporting this interpretation. Hence, the possible erosional remnants of WC rocks are preserved on top of HC rocks in this region. Previous structural geology related research has suggested that the transitional collision of the WC-HC occurred concurrently with the amalgamation of Gondwana, with the WC thrusting over the HC in a NNW–SSE direction (Tani 1997; Kehelpannala 2003; Ranaweera and Kehelpannala 2019). A similar mixed rock zone between these complexes has been identified by Kröner et al. (Kröner et al. 2013a, 2013b) in southern Sri Lanka, where the HC-VC boundary is considered a sub-horizontal thrust zone, with the HC moving eastward atop the VC (Hatherton, Pattaratchi, and Ranasinghe 1975; Vitanage 1985; Kröner et al. 1987a, 1987b, 2013a, 2013b; Voll and Kleinschrodt 1991; Kleinschrodt 1994, 1996; Kriegsman 1995). Most authors suggest that this thrusting of the HC onto the VC occurred during a post-tectonic event, the D3 deformation event as defined by Berger and Jayasinghe (1976), which facilitated the uplift of lower crustal rocks in the HC from lower to middle crust levels. Klippen (outliers) such as Kataragama and Buttala (Figure 1a) in southern HC were displaced over 50 km parallel to the transport direction (e.g., Kriegsman 1995; Voll and Kleinschrodt 1991).

In previous studies, the WC has been characterised as a Neoproterozoic continental arc (Willbold et al. 2004; Kröner, Kehelpannala, and Hegner 2003; Kehelpannala 2004). Santosh et al. (2014) and He et al. (2016) argued that the protoliths of the charnockite in both the HC and WC are arc-related felsic magmatic suites that formed in a Neoproterozoic convergent margin setting. These studies primarily focused on sampling localities in the central and southwestern parts of the two complexes. However, the geochemical signatures of charnockites in the present study suggest that the protoliths of the charnockites in the northeastern part of the WC and HC were formed under two distinct tectonic settings. The WC charnockites in this region were predominantly produced in an extensional tectonic setting, whereas the HC charnockites originated in a subduction-related arc setting. Therefore, a regional-scale geochemical study of charnockite in the Sri Lankan basement is essential to provide a more reliable understanding of the origin of charnockites in this area.

7 | Conclusions

The charnockitic lithologies along the northeastern boundary of the Highland and HC-WC exhibit distinct tectonic signatures, reflecting differentiation into two separate tectonic environments. During the early to middle Neoproterozoic (approximately 1000–720 Ma), the Ferron charnockitic protoliths in the WC were derived from fractionated tholeiitic-type magmas in extensional tectonic settings, within a continental environment. These rocks display metaluminous A2-type compositions.

In contrast, the charnockitic protoliths of the HC were formed from magnesium-rich, metaluminous I-type magmas in a subduction-related arc setting, influenced by calc-alkaline processes.

These tholeiitic and calc-alkaline charnockitic protoliths experienced metamorphism around 610–540 Ma, coinciding with the amalgamation of the Gondwana supercontinent.

The northeastern margin of the HC-WC boundary is a diffused tectonic boundary, where erosional remnants of WC rocks are preserved on top of HC rocks. This is supported by previously published structural geology research, which suggests that during the amalgamation of WC and HC rocks in the Gondwana assembly, the WC was thrust over the HC.

The amalgamation of the WC and HC during the late Neoproterozoic (610–550 Ma) led to the development of granulite- facies metamorphism. Presently, at the erosion surface, the northeastern portion of the HC-WC boundary, particularly around Trincomalee, exhibits a highly diffused nature and manifests as a mixed rock zone.

Acknowledgements

This work was supported by the National Research Council (NRC) Sri Lanka (grant No: NRC 19–092) and the Peradeniya University Research Grant (Grant No. URG/18/43/S). We also acknowledge the Program of the China-Sri Lanka Joint Centre for Water Technology Research and Demonstration by the Chinese Academy of Sciences (CAS) and the China–Sri Lanka Joint Centre for Education and Research by the CAS. The authors acknowledge the support of the National Natural Science Foundation of China (Grant No. W2412091) for the U–Pb zircon geochronology analysis. PLD highly acknowledges the German Academic Exchange Service (DAAD) for the grant DAAD Fellowship for Research Stay for University Academics and Scientists, 2021 (grant no. 5755233). Special thanks are extended to Thilini Harischandra at NIFS, Kandy, and R.K.S. Randunu, Department of Geology, University of Peradeniya, for their support in sample preparation.

Author Contributions

All authors contributed equally.

Conflicts of Interest

The authors declare no conflicts of interest.

Data Availability Statement

The data that supports the findings of this study are available in the Supporting Information of this article.

Peer Review

The peer review history for this article is available at https://www.webofscience.com/api/gateway/wos/peer-review/10.1002/gj.5147.

References

Abewardana, P., S. P. K. Malaviarachchi, P. L. Dharmapriya, A. M. G. K. Wijeratne, and Z. Lei. 2023. "Preliminary Petrology and Major Element Geochemistry of Charnockitic Rocks of the Wanni Complex, Sri Lanka: Implications for Magmatic Relationships." *Journal of the Geological Society of Sri Lanka* 23-2: 23–34.

Ahankoub, M., A. Jahangiri, Y. Asahara, and M. Moayyed. 2013. "Petrochemical and Sr-Nd Isotope Investigations of A-Type Granites in the East of Misho, NW Iran." *Arabian Journal of Geosciences* 6: 4833–4849.

Almond, D. C. 1991. "Arena Gneiss and Kandy Gneiss—A Proposed Subdivision of theHighland Series Around Kandy, and Its Significance." *Journal of the Geological Society of Sri Lanka* 3: 41–50.

Andersen, T. 2002. "Correction of Common Lead in U–Pb Analyses That Do Not Report 204Pb." *Chemical Geology* 192, no. 1–2: 59–79.

Andersen, T., M. A. Elburg, and B. N. Magwaza. 2019. "Sources of Bias in Detrital Zircon Geochronology: Discordance, Concealed Lead Loss and Common Lead Correction." *Earth-Science Reviews* 197: 102899.

Barbarin, B. 1999. "A Review of the Relationships Between Granitoid Types, Their Origins and Their Geodynamic Environments." *Lithos* 46, no. 3: 605–626.

Berger, A. R., and N. R. Jayasinghe. 1976. "Precambrian Structure and Chronology in the Highland Series of Sri Lanka." *Precambrian Research* 3, no. 6: 559–576.

Bonin, B. 2007. "A-Type Granites and Related Rocks: Evolution of a Concept, Problems and Prospects." *Lithos* 97, no. 1–2: 1–29.

Brown, S. J. 1994. *Geology and Geochemistry of the Whakamaru Group Ignimbrites, and Associated Rhyolite Domes*. New Zealand: Taupo Volcanic Zone.

Burton, K. W., and R. K. O'Nions. 1990. "The Timescale and Mechanism of Granulite Formation at Kurunegala, Sri Lanka." *Contributions to Mineralogy and Petrology* 106, no. 1: 66–89.

Busa, T., R. Clochiatti, and R. Cristofolini. 2002. "The Role of Apatite Fractionation and REE Distribution in Alkaline Rocks From Mt. Etna, Sicily." *Mineralogy and Petrology* 74: 95–114.

Cawood, P. A., A. Kroner, and S. Pisarevsky. 2006. "Precambrian Plate Tectonics: Criteria and Evidence." *GSA Today* 16, no. 7: 4.

Chappell, B. W., and A. J. R. White. 1974. "Two Contrasting Granite Types." *Pacific Geology* 8, no. 2: 173–174.

Chappell, B. W., and A. J. R. White. 1992. "I- and S-Type Granites in the Lachlan Fold Belt." *Earth and Environmental Science Transactions of the Royal Society of Edinburgh* 83, no. 1–2: 1–26.

Chin, E. J. 2018. "Deep Crustal Cumulates Reflect Patterns of Continental Rift Volcanism Beneath Tanzania." *Contributions to Mineralogy and Petrology* 173, no. 10: 85.

Condie, K. C., R. D. Hatcher, M. P. Carlson, and J. H. McBride. 2007. "Accretionary Orogens in Space and Time." *Memoir - Geological Society of America* 200: 145.

Condie, K. C., S. A. Pisarevsky, S. J. Puetz, N. M. Roberts, and C. J. Spencer. 2023. "A-Type Granites in Space and Time: Relationship to the Supercontinent Cycle and Mantle Events." *Earth and Planetary Science Letters* 610: 118125.

Cooray, P. G. 1962. "Charnockites and Their Associated Gneisses in the Pre-Cambrian of Ceylon." *Quarterly Journal of the Geological Society* 118, no. 1–4: 239–266.

Cooray, P. G. 1978. "Geology of Sri Lanka." In *Regional Conference on Geology and Mineral Resources of Southeast Asia*, 3, 701–710.

Cooray, P. G. 1982. *Geological Map of Sri Lanka (Ceylon), Scale 1: 500,000*. Colombo, Sri Lanka: Geological Survey Department.

Cooray, P. G. 1984. "Geology, With Special Reference to the Precambrian." In *Ecology and Biogeography in Sri Lanka*, 1–34. Dordrecht: Springer.

Cooray, P. G. 1994. "The Precambrian of Sri Lanka: A Historical Review." *Precambrian Research* 66, no. 1–4: 3–18.

Cordani, U. G., and P. G. Cooray. 1990. "Rb-Sr Ages of Granites and Gneisses From the Precambrian of Sri Lanka." *Journal of the Geological Society of Sri Lanka* 2: 35–43.

Dahanayake, K. 1982. "Structural and Petrological Studies on the Precambrian Vijayan Complex of Sri Lanka." *Revista Brasileira de Geociencias* 12, no. 1–3: 89–93.

Dahanayake, K., and H. A. H. Jayasena. 1983. "General Geology and Petrology of Some Precambrian Crystalline Rocks From the Vijayan Complex of Sri Lanka." *Precambrian Research* 19, no. 3: 301–315.

Dharmapriya, P. L., L. M. Kriegsman, and S. P. Malaviarachchi. 2021. "Spatial Distribution of Ultrahigh-Temperature Granulites of the Highland Complex of Sri Lanka: Lowermost Continental Crust Above an Ultrahot Palaeo-Moho." *Lithos* 404: 106484.

Dharmapriya, P. L., S. P. K. Malaviarachchi, K. Sajeev, and C. Zhang. 2016. "New LA-ICPMS U–Pb Ages of Detrital Zircons From the Highland Complex: Insights Into Late Cryogenian to Early Cambrian (Ca. 665–535 ma) Linkage Between Sri Lanka and India." *International Geology Review* 58, no. 15: 1856–1883.

Dharmapriya, P. L., S. P. K. Malaviarachchi, M. Santosh, L. Tang, and K. Sajeev. 2015. "Late-Neoproterozoic Ultrahigh Temperature Metamorphism in the Highland Complex, Sri Lanka." *Precambrian Research* 271: 311–333.

Dharmapriya, P. L., S. P. Malaviarachchi, A. Galli, et al. 2014. "P–T Evolution of a Spinel+ Quartz Bearing Khondalite From the Highland Complex, Sri Lanka: Implications for Non-UHT Metamorphism." *Journal of Asian Earth Sciences* 95: 99–113.

Dharmapriya, P. L., S. P. Malaviarachchi, A. Galli, et al. 2021. "Hybrid Phase Equilibria Modelling With Conventional and Trace Element Thermobarometry to Assess the P–T Evolution of UHT Granulites: An Example From the Highland Complex, Sri Lanka." *Journal of Metamorphic Geology* 39, no. 2: 209–246.

Dharmapriya, P. L., S. P. Malaviarachchi, L. M. Kriegsman, A. Galli, K. Sajeev, and C. Zhang. 2017b. "New Constraints on the P–T Path of HT/UHT Metapelites From the Highland Complex of Sri Lanka." *Geoscience Frontiers* 8, no. 6: 1405–1430.

Dharmapriya, P. L., S. P. Malaviarachchi, L. M. Kriegsman, et al. 2017a. "Distinct Metamorphic Evolution of Alternating Silica-Saturated and Silica-Deficient Microdomains Within Garnet in Ultrahigh-Temperature Granulites: An Example From Sri Lanka." *Geoscience Frontiers* 8, no. 5: 1115–1133.

Dharmapriya, P. L., S. P. Malaviarachchi, L. M. Kriegsman, et al. 2020. "Symplectite Growth in the Presence of Alkaline Fluids: Evidence From High-Aluminous Metasediments of the Highland Complex, Sri Lanka." *Mineralogy and Petrology* 114, no. 6: 515–538.

Dissanayake, C. B., and T. Munasinghe. 1984. "Reconstruction of the Precambrian Sedimentary Basin in the Granulite Belt of Sri Lanka." *Chemical Geology* 47, no. 3–4: 221–247.

Dunkley, D. J., K. Shiraishi, Y. Motoyoshi, et al. 2014. "Deconstructing the Lützow-Holm Complex With Zircon Geochronology." In *Abstract of 7th International SHRIMP Workshop Program*, 116–121.

Dunkley, D. J., T. Hokada, K. Shiraishi, Y. Hiroi, Y. Nogi, and Y. Motoyoshi. 2020. "Geological subdivision of the Lützow–Holm Complex in East Antarctica: From the Neoarchean to the Neoproterozoic." *Polar Science* 26: 100606.

Eby, G. N. 1990. "The A-Type Granitoids: A Review of Their Occurrence and Chemical Characteristics and Speculations on Their Petrogenesis." *Lithos* 26, no. 1–2: 115–134.

Eby, G. N. 1992. "Chemical Subdivision of the A-Type Granitoids: Petrogenetic and Tectonic Implications." *Geology* 20, no. 7: 641–644.

Elhlou, S., E. Belousova, W. L. Griffin, N. J. Pearson, and S. Y. O'Reilly. 2006. "Trace Element and Isotopic Composition of GJ-Red Zircon Standard by Laser Ablation." *Geochimica et Cosmochimica Acta* 70, no. 18: 158–158.

Forni, F., W. Degruyter, O. Bachmann, G. De Astis, and S. Mollo. 2018. "Long-Term Magmatic Evolution Reveals the Beginning of a New Caldera Cycle At Campi Flegrei." *Science Advances* 4, no. 11: eaat9401.

Frost, B. R., and C. D. Frost. 2008. "A Geochemical Classification for Feldspathic Igneous Rocks." *Journal of Petrology* 49, no. 11: 1955–1969.

Frost, B. R., C. G. Barnes, W. J. Collins, R. J. Arculus, D. J. Ellis, and C. D. Frost. 2001. "A Geochemical Classification for Granitic Rocks." *Journal of Petrology* 42, no. 11: 2033–2048.

Harker, A. 1909. *The Natural History of Igneous Rocks*. Vol. 35, 192. London: Methuen.

Harley, S. L., and N. M. Kelly. 2007. "Zircon Tiny But Timely." *Elements* 3, no. 1: 13–18.

Harris, N. B., J. A. Pearce, and A. G. Tindle. 1986. "Geochemical Characteristics of Collision-Zone Magmatism." *Geological Society, London, Special Publications* 19, no. 1: 67–81.

Hatherton, T., D. B. Pattaratchi, and V. V. C. Ranasinghe. 1975. *Gravity Map of Sri Lanka, 1: 1,000,000, Professional Paper*. Vol. no. 3. Colombo, Sri Lanka: Sri Lanka Geological Survey Department.

He, X. F., M. Santosh, T. Tsunogae, S. P. Malaviarachchi, and P. L. Dharmapriya. 2016. "Neoproterozoic Arc Accretion Along the 'Eastern Suture' in Sri Lanka During Gondwana Assembly." *Precambrian Research* 279: 57–80.

Hirayama, E., T. Tsunogae, S. P. Malaviarachchi, Y. Takamura, P. L. Dharmapriya, and Y. Tsutsumi. 2020. "Prolonged Neoproterozoic High-Grade Metamorphism of the Wanni Complex, Sri Lanka: New Insights From Petrology, Phase Equilibria Modelling, and Zircon U–Pb Geochronology of Partially Melted Cordierite Gneiss From Walpita." *Geological Journal* 55, no. 9: 6147–6168.

Hölzl, S., A. W. Hofmann, W. Todt, and H. Köhler. 1994. "U–Pb Geochronology of the Sri Lanka Basement." In *Tectonic, Metamorphic and Isotopic Evolution of Deep Crustal Rocks, With Special Emphasis on Sri Lanka*, edited by M. Raith and S. Hoernes, vol. 66, 123–149. Precambrian Res.

Hölzl, S., H. Kröner, A. Kröner, P. Jaeckel, and T. C. Liew. 1991. "Geochronology of the Sri Lankan Basement." In *The Crystalline Crust of Sri Lanka, Part-1. Summary of Research of the German-Sri Lankan Consortium*. Geological Survey Department, Sri Lanka, Professional Paper, edited by A. Kröner, vol. 5, 236–257.

Irvine, T. N., and W. R. A. Baragar. 1971. "A Guide to the Chemical Classification of the Common Volcanic Rocks." *Canadian Journal of Earth Sciences* 8, no. 5: 523–548.

Jackson, S. E., N. J. Pearson, W. L. Griffin, and E. A. Belousova. 2004. "The Application of Laser Ablation-Inductively Coupled Plasma-Mass Spectrometry to in Situ U–Pb Zircon Geochronology." *Chemical Geology* 211, no. 1–2: 47–69.

Jacobs, J., S. Pisarevsky, R. J. Thomas, and T. Becker. 2008. "The Kalahari Craton During the Assembly and Dispersal of Rodinia." *Precambrian Research* 160, no. 1–2: 142–158.

Jayathilake, W. M. R., P. L. Dharmapriya, R. Kleinschrodt, and B. Spiering. 2023. "Metamorphic Evolution of Charnockites Across the Inferred Highland-Wanni Boundary in Northeastern Sri Lanka." *Journal of Geological Society of Sri Lanka* 23-I: 34–54.

Jayawardena, D. D. S., and D. A. Carswell. 1976. "The Geochemistry of'charnockites' and Their Constituent Ferromagnesian Minerals From the Precambrian of South-East Sri Lanka (Ceylon)." *Mineralogical Magazine* 40, no. 314: 541–554.

Jiang, X. Y., K. Wu, J. C. Luo, L. P. Zhang, W. D. Sun, and X. P. Xia. 2020. "An A1-Type Granite That Borders A2-Type: Insights From the Geochemical Characteristics of the Zongyang A-Type Granite in the Lower Yangtze River Belt, China." *International Geology Review* 62, no. 17: 2203–2220.

Johansson, Å. 2009. "Baltica, Amazonia and the SAMBA Connection—1000 Million Years of Neighbourhood During the Proterozoic?" *Precambrian Research* 175, no. 1–4: 221–234.

Kehelpannala, K. V. W. 1991. "Structural Evolution of High-Grade Terrains in Sri Lanka With Special Reference to the Areas Around Dodangslanda and Kandy." *Geological Survey Department, Sri Lanka, Professional Paper*, 5, 69–88.

Kehelpannala, K. V. W. 2003. "Structural Evolution of the Middle to Lower Crust in Sri Lanka—A Review." *Journal of the Geological Society of Sri Lanka* 11: 45–85.

Kehelpannala, K. W. 1997. "Deformation of a High-Grade Gondwana Fragment, Sri Lanka." *Gondwana Research* 1, no. 1: 47–68.

Kehelpannala, K. W. 2004. "Arc Accretion Around Sri Lanka During the Assembly of Gondwana." *Gondwana Research* 7, no. 4S: 41–46.

Kehelpannala, K. W., and L. V. Ranaweera. 2007. "Structural and Kinematic Evolution of a Possible Pan-African Suture Zone in Sri Lanka." In *International Association of Gondwana Research Conference Series*, 4, 83–88.

Kelley, K. A., and E. Cottrell. 2009. "Water and the Oxidation State of Subduction Zone Magmas." *Science* 325, no. 5940: 605–607.

King, P. L., A. J. R. White, B. W. Chappell, and C. M. Allen. 1997. "Characterization and Origin of Aluminous A-Type Granites From the Lachlan Fold Belt, Southeastern Australia." *Journal of Petrology* 38, no. 3: 371–391.

Kitano, I., Y. Osanai, N. Nakano, T. Adachi, and I. C. Fitzsimons. 2018. "Detrital Zircon and Igneous Protolith Ages of High-Grade Metamorphic Rocks in the Highland and Wanni Complexes, Sri Lanka: Their Geochronological Correlation With Southern India and East Antarctica." *Journal of Asian Earth Sciences* 156: 122–144.

Kleinschrodt, R. 1994. "Large-Scale Thrusting in the Lower Crustal Basement of Sri Lanka." *Precambrian Research* 66, no. 1–4: 39–57.

Kleinschrodt, R. 1996. "Strain Localization and Large-Scale Block Rotation in the Lower Continental Crust, Kataragama Area, Sri Lanka." *Terra Nova* 8, no. 3: 236–244.

Kleinschrodt, R., G. Voll, and W. Kehelpannala. 1991. "A Layered Basic Intrusion, Deformed and Metamorphosed in Granulite Facies of the Sri Lanka Basement." *Geologische Rundschau* 80, no. 3: 779–800.

Klimm, K., F. Holtz, W. Johannes, and P. L. King. 2003. "Fractionation of Metaluminous A-Type Granites: An Experimental Study of the Wangrah Suite, Lachlan Fold Belt, Australia." *Precambrian Research* 124, no. 2–4: 327–341.

Kriegsman, L. M. 1994. "Evidence for a Fold Nappe in the High-Grade Basement of Central Sri Lanka: Terrane Assembly in the Pan-African Lower Crust?" *Precambrian Research* 66, no. 1–4: 59–76.

Kriegsman, L. M. 1995. "The Pan-African Event in East Antarctica: A View From Sri Lanka and the Mozambique Belt." *Precambrian Research* 75, no. 3–4: 263–277.

Kriegsman, L. M., and J. C. Schumacher. 1999. "Petrology of Sapphirine-Bearing and Associated Granulites From Central Sri Lanka." *Journal of Petrology* 40, no. 8: 1211–1239.

Kröner, A., and I. S. Williams. 1993. "Age of Metamorphism in the High-Grade Rocks of Sri Lanka." *Journal of Geology* 101, no. 4: 513–521.

Kröner, A., I. S. Williams, W. Compston, N. Baur, P. W. Vitanage, and L. R. K. Perera. 1987b. "Zircon Ion Microprobe Dating of High-Grade Rocks in Sri Lanka." *Journal of Geology* 95, no. 6: 775–791.

Kröner, A., K. V. W. Kehelpannala, and E. Hegner. 2003. "Ca. 750–1100 ma Magmatic Events and Grenville-Age Deformation in Sri Lanka: Relevance for Rodinia Supercontinent Formation and Dispersal, and Gondwana Amalgamation." *Journal of Asian Earth Sciences* 22, no. 3: 279–300.

Kröner, A., M. Santosh, and J. Wong. 2012. "Zircon Ages and Hf Isotopic Systematics Reveal Vestiges of Mesoproterozoic to Archaean Crust Within the Late Neoproterozoic–Cambrian High-Grade Terrain of Southernmost India." *Gondwana Research* 21: 876–886.

Kröner, A., P. G. Cooray, and P. W. Vitanage. 1991. "Lithotectonic Subdivision of the Precambrian Basement in Sri Lanka." In *The Crystalline Crust of Sri Lanka, Part-1. Summary of Research of the German-Sri Lankan Consortium*. Geological Survey Department, Sri Lanka, Professional Paper, edited by A. Kröner, vol. 5, 5–21.

Kröner, A., P. Jaeckel, and I. S. Williams. 1994. "Pb-Loss Patterns in Zircons From a High-Grade Metamorphic Terrain as Revealed by Different Dating Methods: U–Pb and Pb–Pb Ages for Igneous and Metamorphic Zircons From Northern Sri Lanka." *Precambrian Research* 66, no. 1–4: 151–181.

Kröner, A., P. Linnebacher, R. J. Stern, T. Reischmann, W. Manton, and I. M. Hussein. 1991. "Evolution of Pan-African Island Arc Assemblages in the Southern Red Sea Hills, Sudan, and in Southwestern Arabia as Exemplified by Geochemistry and Geochronology." *Precambrian Research* 53, no. 1–2: 99–118.

Kröner, A., R. Grieling, T. Reischmann, et al. 1987a. "Pan-African Crustal Evolution in the Nubian Segment of Northeast Africa." *Proterozic Lithospheric Evolution* 17: 235–257.

Kröner, A., Y. Rojas-Agramonte, K. V. W. Kehelpannala, et al. 2013a. "Age, Nd–Hf Isotopes, and Geochemistry of the Vijayan Complex of Eastern and Southern Sri Lanka: A Grenville-Age Magmatic Arc of Unknown Kröner Derivation." *Precambrian Research* 234: 288–321.

Kröner, A., Y. Rojas-Agramonte, K. V. W. Kehelpannala, et al. 2013b. "Age, Nd–Hf Isotopes, and Geochemistry of the Vijayan Complex of Eastern and Southern Sri Lanka: A Grenville-Age Magmatic Arc of Unknown Derivation." *Precambrian Research* 234: 288–321.

Li, C., F. Guo, and W. Fan. 2011. "Lower Crustal Melting Via Magma Underplating: Elemental and Sr–Nd–Pb Isotopic Constraints From Late Mesozoic Intermediate–Felsic Volcanic Rocks in the Northeastern North China Block." *Island Arc* 20, no. 4: 477–499.

Li, Z. X., S. Bogdanova, A. S. Collins, et al. 2008. "Assembly, Configuration, and Break-Up History of Rodinia: A Synthesis." *Precambrian Research* 160, no. 1–2: 179–210.

Liew, T. C., C. C. Milisenda, and A. W. Hofmann. 1991. "Isotopic Contrasts, Chronology of Elemental Transfers and High-Grade Metamorphism: The Sri Lanka Highland Granulites, and the Lewisian (Scotland) and Nuk (SW Greenland) Gneisses." *Geologische Rundschau* 80, no. 2: 279–288.

Loiselle, M. C., and D. R. Wones. 1979. "Characteristics and Origin of Anorogenic Granites." *Abstracts of Papers to Be Presented at the Annual Meetings of the Geological Society of America and Associated Societies, San Diego, California*, 11, 468.

Madhavan, V., K. David, J. Mallikharjuna Rao, N. V. Chalapathi Rao, and M. Srinivas. 1998. "Comparative Study of Lamprophyres From the Cuddapah Intrusive Province (CIP) of Andhra Pradesh, India." *Journal of the Geological Society of India* 52: 621–642.

Malaviarachchi, S. P. 2018. "Review on Age of Magmatism and Crust Formation in Sri Lanka: U–Pb and Lu–Hf Isotopic Perspectives." *Journal of the Indian Institute of Science* 98, no. 4: 417–427.

Malaviarachchi, S. P., and P. L. Dharmapriya. 2015. "Revisiting Ultrahigh Temperature Granulites of Sri Lanka: New Prograde and Retrograde Mineral Textures From the Highland Complex." *Journal of the Indian Institute of Science* 95, no. 2: 159–172.

Malaviarachchi, S. P., and P. L. Dharmapriya. 2021. "Trace Element Ratios Hardly Modify During Extreme Metamorphism of Pelitic Sediments as Evidenced From the Highland Complex, Sri Lanka." *Lithos* 394: 106–120.

Malaviarachchi, S. P., M. Satish-Kumar, and T. Takahashi. 2021. "New Sr-Nd Isotope Data Record Juvenile and Ancient Crust-Mantle Melt Interactions in the Vijayan Complex, Sri Lanka." *Journal of Geology* 129, no. 2: 253.

Manikyamba, C., S. Ganguly, A. Saha, M. Santosh, M. R. Singh, and D. S. Rao. 2014. "Continental Lithospheric Evolution: Constraints From the Geochemistry of Felsic Volcanic Rocks in the Dharwar Craton, India." *Journal of Asian Earth Sciences* 95: 65–80.

Martin, E. L., C. J. Spencer, W. J. Collins, R. J. Thomas, P. H. Macey, and N. M. W. Roberts. 2020. "The Core of Rodinia Formed by the Juxtaposition of Opposed Retreating and Advancing Accretionary Orogens." *Earth-Science Reviews* 211: 103413.

Martin, R. F., D. Schumann, and P. L. Dharmapriya. 2022. "Dolomitic Marble in a Context of Uht Metamorphism: Possible Signs of Melting, Lenadora Quarry, Sri Lanka." *Journal of Petrology* 63, no. 7: egac057.

McDonough, W. F., and S. S. Sun. 1995. "The Composition of the Earth." *Chemical Geology* 120, no. 3–4: 223–253.

Meert, J. G., and T. H. Torsvik. 2003. "The Making and Unmaking of a Supercontinent: Rodinia Revisited." *Tectonophysics* 375, no. 1–4: 261–288.

Middlemost, E. A. 1994. "Naming Materials in the Magma/Igneous Rock System." *Earth-Science Reviews* 37, no. 3–4: 215–224.

Milisenda, C. C., T. C. Liew, A. W. Hofmann, and A. Kröner. 1988. "Isotopic Mapping of Age Provinces in Precambrian High-Grade Terrains: Sri Lanka." *Journal of Geology* 96, no. 5: 608–615.

Milisenda, C. C., T. C. Liewa, A. W. Hofmanna, and H. Köhler. 1994. "Nd Isotopic Mapping of the Sri Lanka Basement: Update, and Additional Constraints From Sr Isotopes." *Precambrian Research* 66, no. 1–4: 95–110.

Munasinghe, T., and C. Dissanayake. 1980. "Are Charnockites Metamorphosed Archean Volcanic Rocks? A Case Study From Sri Lanka." *Precambrian Research* 12, no. 1–4: 459–470.

Osanai, Y., K. Sajeev, M. Owada, et al. 2006. "Metamorphic Evolution of Ultrahigh-Temperature and High Pressure Granulites From Highland Complex, Sri Lanka." *Journal of Asian Earth Sciences* 28: 20–37.

Osanai, Y., K. Sajeev, N. Nakano, et al. 2016. "UHT Granulites of the Highland Complex, Sri Lanka I: Geological and Petrological Background." *Journal of Mineralogical and Petrological Sciences* 111, no. 3: 145–156.

Pearce, J. A., N. B. Harris, and A. G. Tindle. 1984. "Trace Element Discrimination Diagrams for the Tectonic Interpretation of Granitic Rocks." *Journal of Petrology* 25, no. 4: 956–983.

Perera, L. R. K., and H. Kagami. 2011. "Centimetre-and Metre-Scale Nd and Sr Isotopic Homogenization in Kadugannawa Complex, Sri Lanka." *Journal of the Geological Society of Sri Lanka* 14: 129–141.

Pitawala, A., M. Schidlowski, K. Dahanayake, and W. Hofmeister. 2003. "Geochemical and Petrological Characteristics of Eppawala Phosphate Deposits, Sri Lanka." *Mineralium Deposita* 38: 505–515.

Pohl, J. G., and R. Emmermann. 1991. "Chemical Composition of the Sri Lanka Precambrian Basement." In *The Crystalline Crust of Sri Lanka, Part I. Summary of Research of the German–Sri Lankan Consortium, Geological Survey. Department Sri Lanka, Professional Paper*, edited by A. Kröner, vol. 5, 94–123. Sri Lanka: Geological Survey Department.

Pram, W. K. B. N., and J. Pohl. 1994. "Geochemistry of Pelitic and Psammopelitic Precambrian Metasediments From Southwestern Sri Lanka: Implications for Two Contrasting Source-Terrains and Tectonic Settings." *Precambrian Research* 66, no. 1–4: 223–244.

Prame, N. 1997. "Geochemistry and Genesis of Granitoid Rocks From Southern Sri Lanka." *Mineralogy and Petrology* 60, no. 3–4: 245.

Raase, P., and V. Schenk. 1994. "Petrology of Granulite-Facies Metapelites of the Highland Complex, Sri Lanka: Implications for the Metamorphic Zonation and the PT Path." *Precambrian Research* 66, no. 1–4: 265–294.

Ranaweera, L. V. 2008. "*The Wanni-Highland Boundary Shear Zone of Sri Lanka: Field and Structural Evidence*." Doctoral dissertation.

Ranaweera, L. V., and K. W. Kehelpannala. 2019. "Mesoscopic to Microcropic Structures Associated With the Wanni Complex/Highland Complex Boundary Shear Zone in Sri Lanka." *Journal of the Geological Society of Sri Lanka* 20, no. 2: 1.

Ratheesh-Kumar, R. T., P. L. Dharmapriya, B. F. Windley, W. J. Xiao, and U. Jeevan. 2020. "The Tectonic 'Umbilical Cord' Linking India and Sri Lanka and the Tale of Their Failed Rift. Journal of Geophysical Research: Solid." *Earth* 125, no. 5: e2019JB018225.

Roberts, N. M., and T. Slagstad. 2015. "Continental Growth and Reworking on the Edge of the Columbia and Rodinia Supercontinents; 1.86–0.9 Ga Accretionary Orogeny in Southwest Fennoscandia." *International Geology Review* 57, no. 11–12: 1582–1606.

Rubatto, D. 2017. "Zircon: The Metamorphic Mineral." *Reviews in Mineralogy and Geochemistry* 83, no. 1: 261–295.

Rubatto, D., and J. Hermann. 2003. "Zircon Formation During Fluid Circulation in Eclogites (Monviso, Western Alps): Implications for Zr and Hf Budget in Subduction Zones." *Geochimica et Cosmochimica acta* 67, no. 12: 2173–2187.

Rudnick, R. L. 1992. "Restites, Eu Anomalies and the Lower Continental Crust." *Geochimica et Cosmochimica Acta* 56, no. 3: 963–970.

Sajeev, K., and Y. Osanai. 2004a. "Osumilite and Spinel+ Quartz From Sri Lanka: Implications for UHT Conditions and Retrograde PT Path." *Journal of Mineralogical and Petrological Sciences* 99, no. 5: 320–327.

Sajeev, K., and Y. Osanai. 2004b. "Ultrahigh-Temperature Metamorphism (1150 C, 12 kbar) and Multistage Evolution of mg-, Al-Rich Granulites From the Central Highland Complex, Sri Lanka." *Journal of Petrology* 45, no. 9: 1821–1844.

Sajeev, K., I. S. Williams, and Y. Osanai. 2010. "Sensitive High-Resolution Ion Microprobe U–Pb Dating of Prograde and Retrograde Ultrahigh-Temperature Metamorphismas Exemplified by Sri Lankan Granulites." *Geology* 38: 971–974.

Sajeev, K., Y. Osanai, J. A. D. Connolly, et al. 2007. "Extreme Crustal Metamorphism During a Neoproterozoic Event in Sri Lanka: A Study of Dry Mafic Granulites." *Journal of Geology* 115, no. 5: 563–582.

Santosh, M., C. N. Hu, X. F. He, et al. 2017. "Neoproterozoic Arc Magmatism in the Southern Madurai Block, India: Subduction, Relamination, Continental Outbuilding, and the Growth of Gondwana." *Gondwana Research* 45: 1–42.

Santosh, M., T. Tsunogae, S. P. Malaviarachchi, et al. 2014. "Neoproterozoic Crustal Evolution in Sri Lanka: Insights From Petrologic, Geochemical and Zircon U–Pb and Lu–Hf Isotopic Data and Implications for Gondwana Assembly." *Precambrian Research* 255: 1–29.

Satish-Kumar, M., M. Shirakawa, A. Imura, et al. 2021. "A Geochemical and Isotopic Perspective on Tectonic Setting and Depositional Environment of Precambrian Meta-Carbonate Rocks in Collisional Orogenic Belts." *Gondwana Research* 96: 163–204.

Sen, G., and R. J. Stern. 2021. "Subduction Zone Magmas." *Encyclopedia of Geology* 2: 33–51.

Shand, S. J. 1948. "Eruptive Rocks." (Vol. 66, No. 1, p. 78). LWW.

Shearer, C. K., and J. J. Papike. 1989. "Is Plagioclase Removal Responsible for the Negative Eu Anomaly in the Source Regions of Mare Basalts?" *Geochimica et Cosmochimica Acta* 53, no. 12: 3331–3336.

Shellnutt, J. G., and M. F. Zhou. 2007. "Permian Peralkaline, Peraluminous and Metaluminous A-Type Granites in the Panxi District, SW China: Their Relationship to the Emeishan Mantle Plume." *Chemical Geology* 243, no. 3–4: 286–316.

Shiraishi, K., D. J. Ellis, Y. Hiroi, C. M. Fanning, Y. Motoyoshi, and Y. Nakai. 1994. "Cambrian Orogenic Belt in East Antarctica and Sri Lanka: Implications for Gondwana Assembly." *Journal of Geology* 102, no. 1: 47–65.

Shiraishi, K., T. Hokada, C. M. Fanning, K. Misawa, and Y. Motoyoshi. 2003. "Timing of Thermal Events in Eastern Dronning Maud Land, East Antarctica." *Polar Geoscience* 16: 76–99.

Su, B. X., J. Wang, M. M. Cui, et al. 2022. "Element Partitioning and Li-O Isotope Fractionation Between Silicate Minerals and Crustal-Derived Carbonatites and Their Implications." *Journal of Geophysical Research: Solid Earth* 127, no. 6: e2022JB024563.

Sun, S. S., and W. F. McDonough. 1989. "Chemical and Isotopic Systematics of Oceanic Basalts: Implications for Mantle Composition and Processes." *Geological Society, London, Special Publications* 42, no. 1: 313–345.

Survey Department of Sri Lanka. 2007. *National Atlas of Sri Lanka*. 2nd ed, 243. Colombo, Sri Lanka: Survey Department of Sri Lanka.

Takahashi, K., T. Tsunogae, M. Santosh, Y. Takamura, and Y. Tsutsumi. 2018. "Paleoproterozoic (ca. 1.8 Ga) Arc Magmatism in the Lützow-Holm Complex, East Antarctica: Implications for Crustal Growth and Terrane Assembly in Erstwhile Gondwana Fragments." *Journal of Asian Earth Sciences* 157: 245–268.

Takamura, Y., T. Tsunogae, M. Santosh, S. P. Malaviarachchi, and Y. Tsutsumi. 2016. "U–Pb Geochronology of Detrital Zircon in Metasediments From Sri Lanka: Implications for the Regional Correlation of Gondwana Fragments." *Precambrian Research* 281: 434–452.

Tani, Y. 1997. "A Preliminary Study of the Deformational Structures and." *Journal of Geosciences. Osaka City University* 40: 51–67.

Tani, Y., and M. Yoshida. 1996. "The Structural Evolution of the Arena Gneisses and Its Bearing on Proterozoic Tectonics of Sri Lanka." *Journal of Southeast Asian Earth Sciences* 14, no. 3–4: 309–329.

Tsunogae, T., D. J. Dunkley, K. Horie, T. Endo, T. Miyamoto, and M. Kato. 2014. "Petrology and SHRIMP Zircon Geochronology of Granulites From Vesleknausen, Lützow-Holm Complex, East Antarctica: Neoarchean Magmatism and Neoproterozoic High-Grade Metamorphism." *Geoscience Frontiers* 5, no. 2: 167–182.

Tsunogae, T., Q. Y. Yang, and M. Santosh. 2015. "Early Neoproterozoic Arc Magmatism in the Lützow-Holm Complex, East Antarctica: Petrology, Geochemistry, Zircon U–Pb Geochronology and Lu–Hf Isotopes and Tectonic Implications." *Precambrian Research* 266: 467–489.

Tsunogae, T., Q. Y. Yang, and M. Santosh. 2016. "Neoarchean–Early Paleoproterozoic and Early Neoproterozoic Arc Magmatism in the Lützow–Holm Complex, East Antarctica: Insights From Petrology, Geochemistry, Zircon U–Pb Geochronology and Lu–Hf Isotopes." *Lithos* 263: 239–256.

Vermeesch, P., and V. Pease. 2021. "A Genetic Classification of the Tholeiitic and Calc-Alkaline Magma Series." *Geochemical Perspectives Letters* 19: 1–6.

Vitanage, P. W. 1959. "Geology of the Country around Polonnaruwa." Professional paper No 1, Geological Survey Department, Sri Lanka, 75.

Vitanage, P. W. 1972. "Post-Precambrian Uplifts and Regional Neotectonic Movements in Ceylon." *Proceedings 24th IGC*, 642–654.

Vitanage, P. W. 1985. "The Geology, Structure and Tectonics of Sri Lanka and South India." *Publication Occasionnelle-Centre International Pour la Formation et les échanges géologiques* 6: 5–15.

Voll, G., and R. Kleinschrodt. 1991. "Sri Lanka: Structural, Magmatic and Metamorphic Development of a Gondwana Fragment." *Crystalline Crust of Sri Lanka* 1: 22–51.

Wang, G. G., P. Ni, A. D. Zhu, et al. 2018. "1.01–0.98 Ga Mafic Intra-Plate Magmatism and Related Cu-Au Mineralization in the Eastern Jiangnan Orogen: Evidence From Liujia and Tieshajie Basalts." *Precambrian Research* 309: 6–21.

Wang, J., B. X. Su, C. Chen, et al. 2021. "Crustal Derivation of the Ca. 475 ma Eppawala Carbonatites in Sri Lanka." *Journal of Petrology* 62, no. 11: egab075.

Wang, R. C., L. Xie, J. Chen, et al. 2013. "Tin-Carrier Minerals in Metaluminous Granites of the Western Nanling Range (Southern China): Constraints on Processes of Tin Mineralization in Oxidized Granites." *Journal of Asian Earth Sciences* 74: 361–372.

Whalen, J. B., K. L. Currie, and B. W. Chappell. 1987. "A-Type Granites: Geochemical Characteristics, Discrimination and Petrogenesis." *Contributions to Mineralogy and Petrology* 95, no. 4: 407–419.

Whitehouse, M. J., B. S. Kamber, and S. Moorbath. 1999. "Age Significance of U–Th–Pb Zircon Data From Early Archaean Rocks of West Greenland—A Reassessment Based on Combined Ion-Microprobe and Imaging Studies." *Chemical Geology* 160, no. 3: 201–224.

Wickremasinghe, O. C. 1969. "*The Geochemistry and Geochronology of the Charnockites and Associated Rocks of Ceylon*." Doctoral dissertation, University of Leeds (Department of Earth Sciences).

Wiedenbeck, M. 1995. "An Example of Reverse Discordance During Ion Microprobe Zircon Dating: An Artifact of Enhanced Ion Yields From a Radiogenic Labile Pb." *Chemical Geology* 125, no. 3–4: 197–218.

Willbold, M., E. Hegner, R. Kleinschrodt, H. G. Stosch, K. V. W. Kehelpannala, and P. Dulski. 2004. "Geochemical Evidence for a Neoproterozoic Magmatic Continental Margin in Sri Lanka—Relevance for the Rodinia–Gondwana Supercontinent Cycle." *Precambrian Research* 130, no. 1–4: 185–198.

Xie, L., Y. Zhang, H. Zhang, J. Sun, and F. Wu. 2008. "In Situ Simultaneous Determination of Trace Elements, U-Pb and Lu-Hf Isotopes in Zircon and Baddeleyite." *Chinese Science Bulletin* 53: 1565–1573.

Yakymchuk, C., C. L. Kirkland, and C. Clark. 2018. "Th/U Ratios in Metamorphic Zircon." *Journal of Metamorphic Geology* 36, no. 6: 715–737.

Yoshida, M. 1978. "Tectonics and Petrology of Charnockites Around Lutzow-Holmbukta." *Journal of Geosciences. Osaka City University* 21: 65–152.

Yoshida, M. 1979. "Metamorphic Conditions of the Polymetamorphic Lützow-Holmbukta Region, East Antarctica." *Journal of Geosciences. Osaka City University* 22: 97–140.

Zhang, D., and A. Audétat. 2017. "What Caused the Formation of the Giant Bingham Canyon Porphyry Cu-Mo-Au Deposit? Insights From Melt Inclusions and Magmatic Sulfides." *Economic Geology* 112, no. 2: 221–244.

Zhao, L., P. L. Dharmapriya, Y. B. Zhang, et al. 2023. "Expanding Azania at the Heart of Gondwana: Terrane Correlation From Southern India to Sri Lanka." *Precambrian Research* 395: 107149.

Zimmer, M. M., T. Plank, E. H. Hauri, et al. 2010. "The Role of Water in Generating the Calc-Alkaline Trend: New Volatile Data for Aleutian Magmas and a New Tholeiitic Index." *Journal of Petrology* 51, no. 12: 2411–2444.

Supporting Information

Additional supporting information can be found online in the Supporting Information section.